Chapter 5

Magnetic Particles

The first approach presented used conductive materials to create a target, which would be applied to the pipe surface after manufacturing. An alternative approach would be to incorporate a material directly into the pipe material, to make the polyethylene intrinsically detectable. Preliminary work was done to incorporate magnetic materials into polyethylene, which could then render the pipe detectable with a metal detector. This work was based on previous work by GTI, which demonstrated that polyethylene pipes doped with a high percentage of magnetic powder could be detectable at depths of three to five feet [38]. However, the magnetic powders used by GTI contained costly materials made from heavy metals, and so this work aims to reproduce some of these results using less expensive and more environmentally-friendly materials.

Two types of magnetic materials were considered as additives. Magnetic Ink Character Recognition (MICR) toner is ink mixed with iron oxide particles, and is

most commonly used to print numbers that can be read by computer at the bottom of checks. MICR toner can be purchased and used as received. A second material, synthesized iron nanoparticles, are formed by mixing iron(II) chloride and iron(III) chloride with ammonium hydroxide to form magnetite. Because these particles are a form of iron oxide, they have a stronger magnetic response than the MICR toner. Over time, though, these particles will oxidize and become maghemite, which is a less magnetic form of iron oxide [21]. Because polyethylene is a thermoplastic, the molding process requires elevated temperatures, which are known to accelerate iron oxidation.

5.1 Magnetic Scans of Materials in Polyethylene

For magnetic particles to represent a feasible long term solution for pipe location, the particles must remain magnetic over time. An equal weight of magnetic nanoparticles and MICR ink were each mixed into a polyethylene plate and scanned with a magnetic scanning system [37] to determine which had a stronger magnetic response in the polyethylene. Both plates were scanned again after a period of six months to determine if the magnetic response had any decrease over time. The magnetic scans of the MICR in polyethylene are shown in Figure 5.1 and the magnetic scans of the iron nanoparticles in polyethylene are shown in Figure 5.2.

Using ImageJ, the background magnetic response was filtered out, leaving only the areas of the magnetic response, which could be measured to determine the difference in the magnetic response before and after the six month period. The

Table 5.1: Pixel counts from ImageJ of the magnetic areas from the filtered before and after images from the magnetic scans.

	Initial	Six Months	Percent Difference
MICR Toner	2246	2426	8.014%
IONP	34670	8866	-74.43%

pixel counts and percent differences are shown in Table 5.1.

The iron nanoparticles have a stronger magnetic response than an equivalent weight of the MICR toner both initially and after the six month period. In Figure 5.2, the concentrations of the magnetic particles are strongest around the edges of the polyethylene disk, and this can be seen in the magnetic scan images and the photograph of the disk. In the polyethylene with the MICR toner, the shape of the disk can not be seen as clearly in the magnetic scans. However, the strength of the magnetic response of the iron nanoparticles decreased significantly over the six months between the initial and final scan, indicating that the iron particles have oxidized, but the scan of the MICR toner had about the same magnitude both before and after the six months.

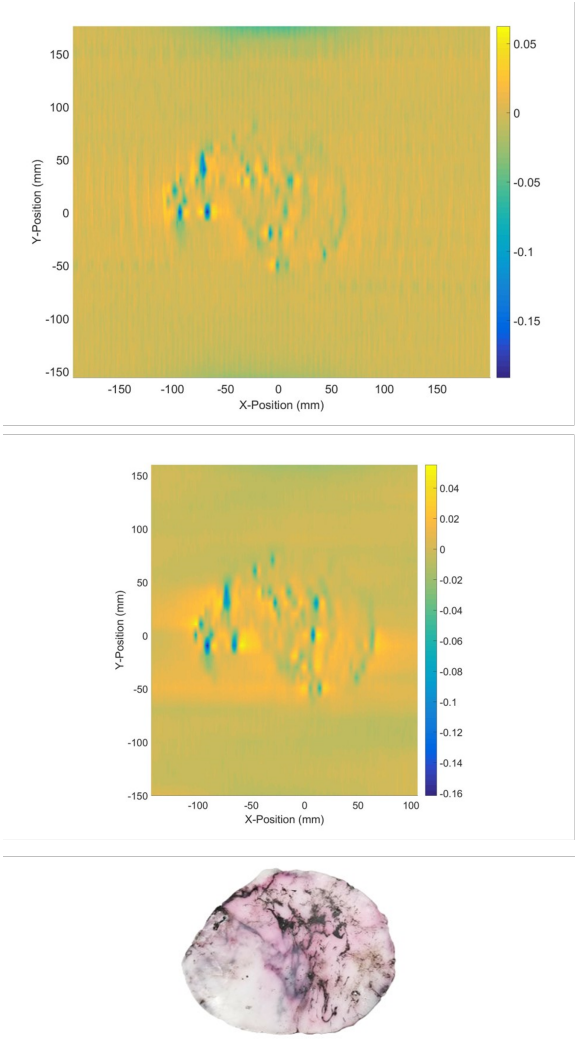

Figure 5.1: Before-and-after magnetic scans of MICR toner mixed into polyethylene. (Top) Immediately after manufacturing (Middle) Six months after manufacturing (Bottom) The specimen that was scanned.

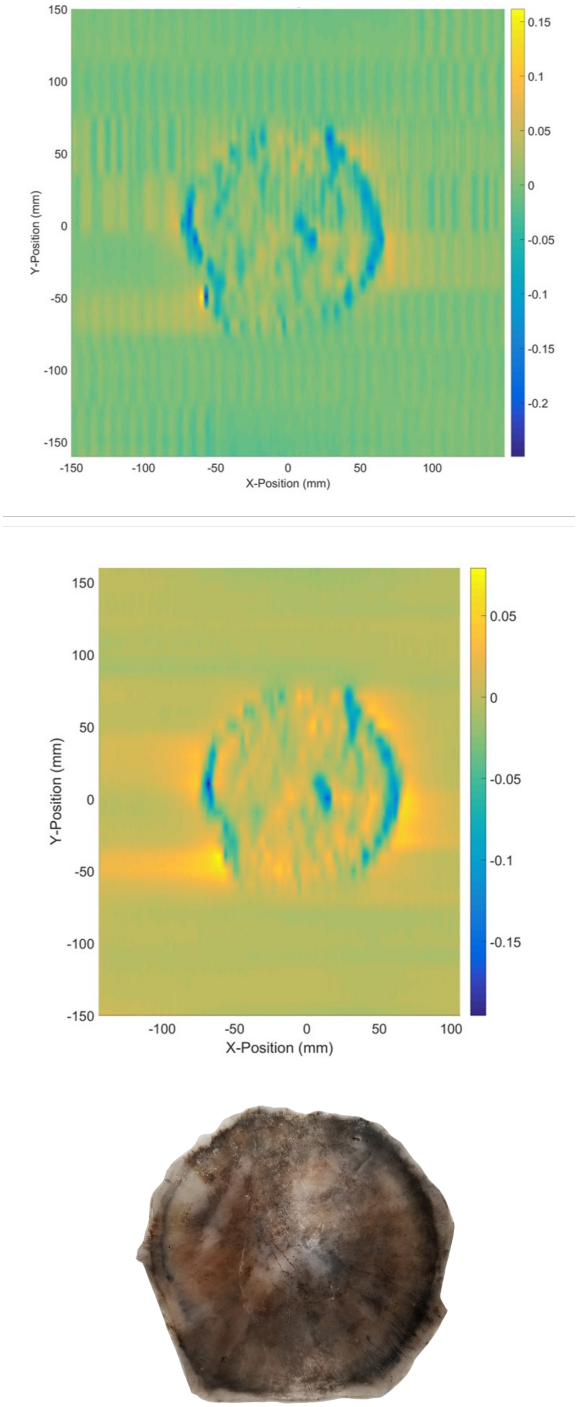

Figure 5.2: Before-and-after magnetic scans of iron nanoparticles mixed into polyethylene. (Top) Immediately after manufacturing (Middle) Six months after manufacturing (Bottom) The specimen that was scanned.

5.2 Encapsulation

Even at room temperature, the iron nanoparticles are known to oxidize over time, reducing the magnetic strength of the particles. If the particles can be protected from oxidation, they will retain a stronger magnetic response for a longer period of time. One method of protecting the nanoparticles from the high temperatures experienced during the molding process is encapsulation. Nanoparticles or MICR toner were mixed into a core material, and then encapsulated into urea-formaldehyde capsules [19]. In this case, the core material was chosen to be dibutyl phthalate (DBP), because it has a boiling point higher than the temperatures expected during polyethylene processing and is very nonpolar, which is ideal for this encapsulation process. Capsules without and with magnetic core material are shown in Figure 5.3.

5.3 Size Distribution of Capsules

Compounds are traditionally mixed into polyethylene through high shear processes, such as a twin-screw or Banbury mixer, or roller mills. Polyethylene pipes are manufactured through extrusion. Both of these processes involve high forces in addition to high temperatures, which are likely to crush microcapsules that are used as additives. Capsules with smaller diameters are more likely to survive; the encapsulation process produces capsules of relatively constant wall thickness regardless of capsule diameter, so smaller capsules will have a higher ratio of wall thickness to diameter.

The capsule manufacturing process involves agitation of the core liquid and the

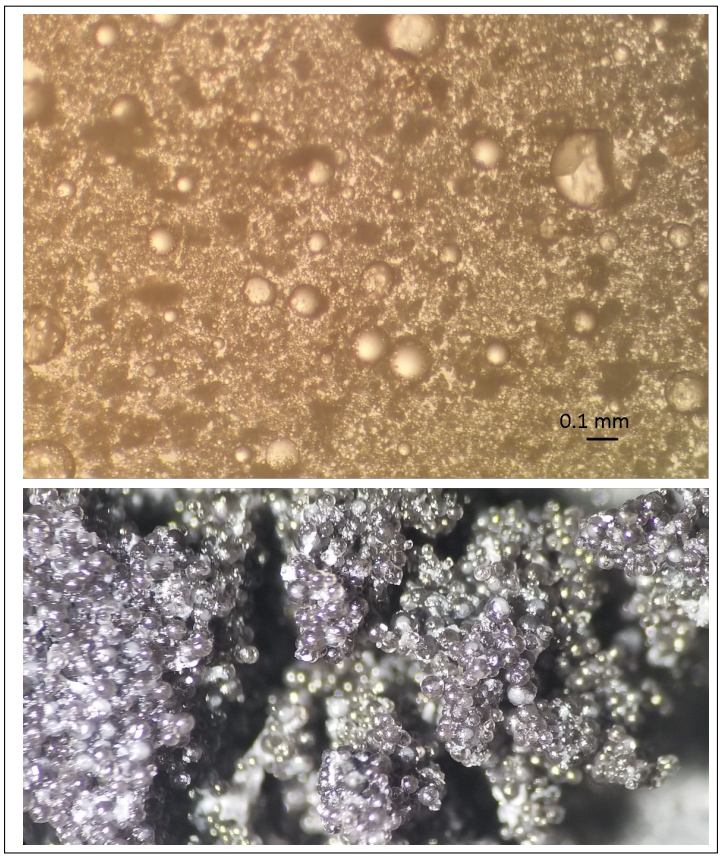

Figure 5.3: (Top) Urea/Formaldehyde microcapsules with a core of dibutyl phthalate. (Bottom) Urea/Formaldehyde microcapsules with a core of dibutyl phthalate and MICR toner.

shell solution in a water bath. Varying the speed of the immersion mixer will alter the size of the capsules that are produced. If the bath is mixed faster, there is more energy in the system, and the core and shell droplets will break up, resulting in smaller capsules. More energy can be added to the system by adding a high shear step to the process called homogenization, which reduces the size of the core droplets even further.

Multiple batches of capsules were created with varying mechanical parameters. A sample of microcapsules from each batch was imaged under a microscope, and the capsules in each image were measured with ImageJ to gain a size distribution for the capsules. Table 5.2 shows average capsule diameter and standard deviation for each batch of microcapsules.

Without homogenization, a higher mixer speed would result in smaller capsules. However, when homogenization was added to the process, the higher rate of agitation would cause the droplets in solution to collide, resulting in capsules that were larger on average and had a wider size distribution [12]. The smallest capsules produced (Batch 9 in Table 5.2) were created through the lowest mixer and homogenizer speeds, and were homogenized for the longest period of time.

The smallest capsules were examined with the Scanning Electron Microscope. At such high magnifications, it could be seen that some of the capsules were bowl shaped, as seen in Figure 5.4, which is not seen in larger capsules. The shells are also much smoother than those of the larger capsules [21].

Table 5.2: Effect of Mechanical Mixing Parameters on Microcapsule Size

Batch Number	1	2	3	4	5	6	7	8	9
Dodecane Amount	0%	5%	5%	5%	5%	5%	5%	5%	5%
Mixer Speed (RPM)	500	500	500	500	500	1000	200	500	200
Homogenizer Speed	3	3	3	1	3	3	3	5	1
Homogenizer Time (minutes)	10	10	20	10	5	10	10	10	20
Mean Diameter (μmeter)	2.24	2.12	1.69	1.58	3.37	4.50	1.44	2.65	1.07
Standard Deviation (μmeter)	0.96	1.15	0.66	0.73	1.48	3.19	0.48	1.23	0.41

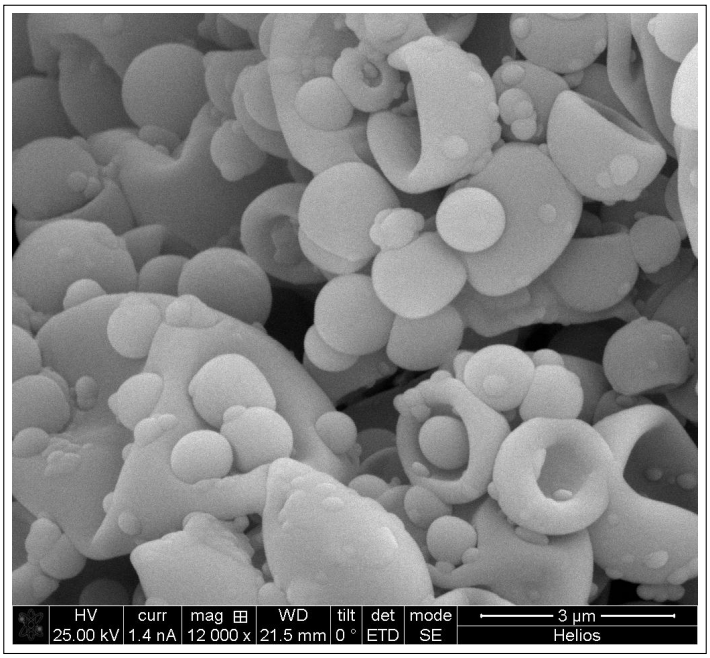

Figure 5.4: Urea/Formaldehyde microcapsules as seen with a Scanning Electron Microscope.

5.4 Survivability of Microcapsules

To determine if the capsules could survive the polyethylene molding process, capsules were molded into polyethylene plates at 180°C. The resulting plates were cross sectioned and the section surfaces were examined for evidence of capsules. For capsules without homogenization, which had diameters of 100 μm, no evidence of capsules could be found. However, for the smallest capsules with diameters of 5 μm, capsules both intact and crushed were found. Examples of these capsules are shown in Figure 5.5.

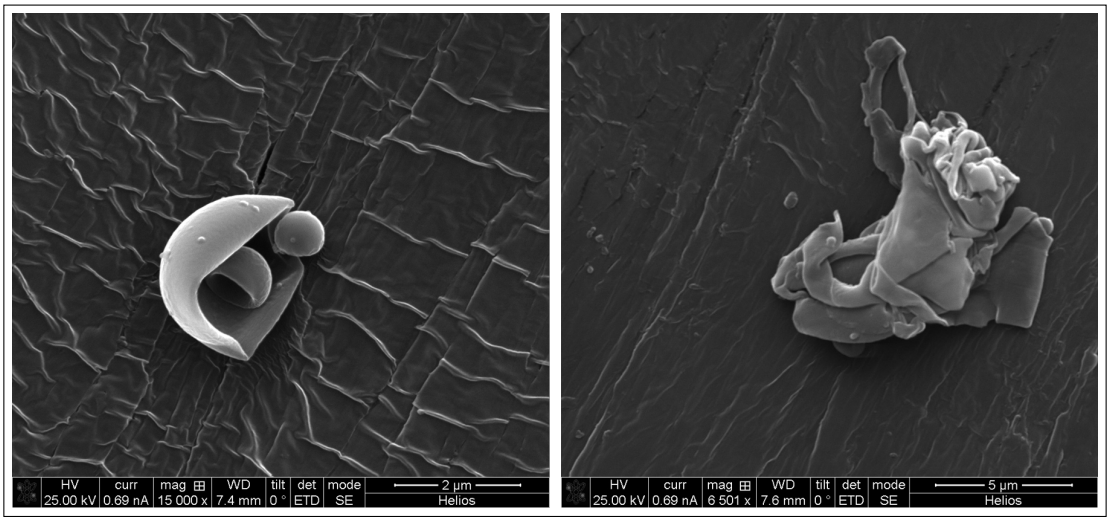

Figure 5.5: (Left) SEM image of microcapsules which survived the molding process in polyethylene. (Right) A microcapsule which was crushed during molding.

However, more evidence of microcapsules was expected. Using stronger capsules, like dopamine-coated double-walled capsules [35], could increase the chance of these capsules surviving the high heat and pressure of the molding processes.

5.4.1 Future Work

To this point, only preliminary work has been done using this approach. Capsule survivability studies should continue, using the stronger capsules. Capsules will be mixed into the polyethylene using the Banbury mixer, which has higher shear than the compression molding setup that is used currently.

Studies have been done that quantify the amount of iron nanoparticles that can be successfully encapsulated [21]. This data can be used to define how many microcapsules should be compounded into polyethylene such that it becomes detectable with a metal detector.

Adding quantities of capsules to the polyethylene will change its material properties, and so mechanical testing should be done on the capsule-laden polyethylene.

Chapter 6

Tag Fabrication, and Simulation

In order to create these previously mentioned time delay tags, these have to be both made in a cost effective manner and be able to be simulated with common electromagnetic software. The software used here will be ANSYS HFSS in order to identify potential tag candidates for manufacture and experimentation. In this project there were two approaches to fabricating antennas for further analysis. A conductive polyethylene approach, where a new conductive PE material was synthesized and a metal foil technique that allowed for the exploration of various

6.1 Manufacturing Metallic Test Tags

Most microwave transmission designs on a substrate are typically microstrips, using one conductor and one ground plane with a substrate of fiberglass, loaded dielectric plastic or ceramic in the middle. An alternative to microstrips is using CPWs without a ground plane underneath using a flexible substrate, like fabrics or thin

plastic sheets, in order to conform to the shape of an object. These RF circuits would also normally be created on a rigid substrate like fiberglass too, but this does accommodate itself when trying to conform a tag to a pipe. Instead these tags can be created on other more flexible fabrics or thinner plastics.

The tags are cut out from aluminum foil with a thickness of approximately 0.035 mm with a Silhouette Cameo adhered on top of 1/32-inch HDPE sheet. Normally, HDPE does not accept adhesives, but with a simple flame or plasma treatment, adhesives properly bond to polyethylene (PE). If construction details are small enough, where the cutting plotter might tear the foil when on plastic, the tag substrate was replaced with paper instead and then placed on or between the plastic. Excess foil is manually removed with a blade. When small tears occur on the CPW, small pieces of copper tape is placed and shaped over the line. This fix is then verified with a simple conductivity test with a probe on each side of the repaired line. Fabricating HDPE pipes with attached delay lines would then require that the antenna be attached using either hot pressing or adhesives, however this is outside of the main scope and will require further research. In manufacturing, the gap between the conductor and ground plane increased as reflected in the fourth column of Table 6.2 where the gap is 1 mm instead of the simulated 0.5 mm. With a short enough length of transmission line, the gap and width do not matter as much when simulating these antennas. These transmission lines more act as a reliable method to insert lumped ports when solving a driven modal solution in HFSS as a single port. Although the transmission line with a larger gap will radiate more, the larger gap also affords more flexibility with the types of dielectrics that are around it.

Table 6.1: Cost breakdown of each dumb tag.

Item	Uses	Cost ($)	Single Use Cost ($)
Silhouette Cameo	1000	200.00	0.20
Silhouette Blades	25	10.00	0.40
4'x8' 1/32" HDPE sheet	32	19.56	0.61
Aluminum Foil (1'x500')	500	36.10	0.07
Spray on adhesive	30	13.71	0.46
Butane torch	100	20.00	0.20
Total			1.94

In addition to the foil transmission lines tags, simple shapes like bowtie antennas can be easily cut out and be connected directly to each other to form a double bowtie tag. If the shape does not have much complexity, it can be spray painted on with conductive paint and a negative of a tag as noted by Thompson when making a reflector dish [59]. The concerning factor with spray paint is if the paint is thick enough to meet skin effect criterion for that specific frequency. All tags mentioned before were created and displayed in Fig. 7.6 and a simple cost breakdown of each tag is included in 6.1.

6.2 Transmission Line Simulation

To create the single layer CPWs, the cutting plotter technique becomes the easiest and cheapest option. Aluminum foil, instead of more expensive copper foil, is used to either adhere to a plastic or paper sheet. The phase velocity and impedance of these two lines are both proportional to the average effective dielectric constant where the speed in the transmission lines is in Eq. 2.2.

Any dielectric material will change transmission line characteristics, where the overall dielectric, simplified, is the average between air and the substrate. If a tag is placed underground on top of a pipe, the dielectric constant is then the average between the pipe and the soil. To pack larger lengths of transmission line into a smaller space, this CPW transmission line uses 90° turns that have a radius 4 times larger than the width of the CPW, since as Pozar notes for microstrips, the radius has to be at least three times larger than the width of the conductor [48]. The width of the conductor is 1 mm and the gap between the conductor and the ground plane is 0.1 mm. Table 6.2 reviews the impedance of several variations of a CPW in free space, between PVC and HDPE and between a HDPE pipe and clay with a dielectric constant of 16 along with noting the simulated antenna impedance for a UWB planar circular antenna. This table also notes the effective velocity factor (VF) in these transmission lines and the appropriate delay on the transmission line over 660 mm with an open circuit termination. Fig. 6.1 shows the simulation results in several different environments with open and closed circuit terminations in order to produce varying reflections. The short transmission line, thus, delays the signal by 2 ns and the long transmission line delays the signal by 4 ns in free space. The short termination at the end of the transmission line inverts the pulse while the open termination keeps the same pulse shape. Because the impedance of the CPW will not always be 50Ω, it produces extra spurious reflections, due to simulation port impedance of 50Ω. The transmission line should act similarly when mismatched to the antenna.

Table 6.2: Reflection parameters and velocity factors for transmission lines and antennas simulated in three dielectric environments and three varying sizes of CPWs with (a) w=1 mm s=0.1 mm, (b) w=1 mm s=0.5 mm and (c) w=1 mm s=1 mm with a length of 660 mm with an open circuit termination.

	Z_0 at 600 MHz					
Environment	(a)	(b)	(c)	Antenna	VF	Delay(ns)
Free Space	$41 - 16j\Omega$	$52 + 11j\Omega$	$53 + 17.5j\Omega$	$38.5 + 8.5j\Omega$	1	4.5
PVC/HDPE	$24.5 - 21j\Omega$	$52\Omega + 4j\Omega$	$56 + 15.5j\Omega$	$53.5 + 12j\Omega$	0.63	7
HDPE/Clay	$4 - 9j\Omega$	$20.5 - 14j\Omega$	$35.5 - 9j\Omega$	$41 - 7.5j\Omega$	0.33	13.5

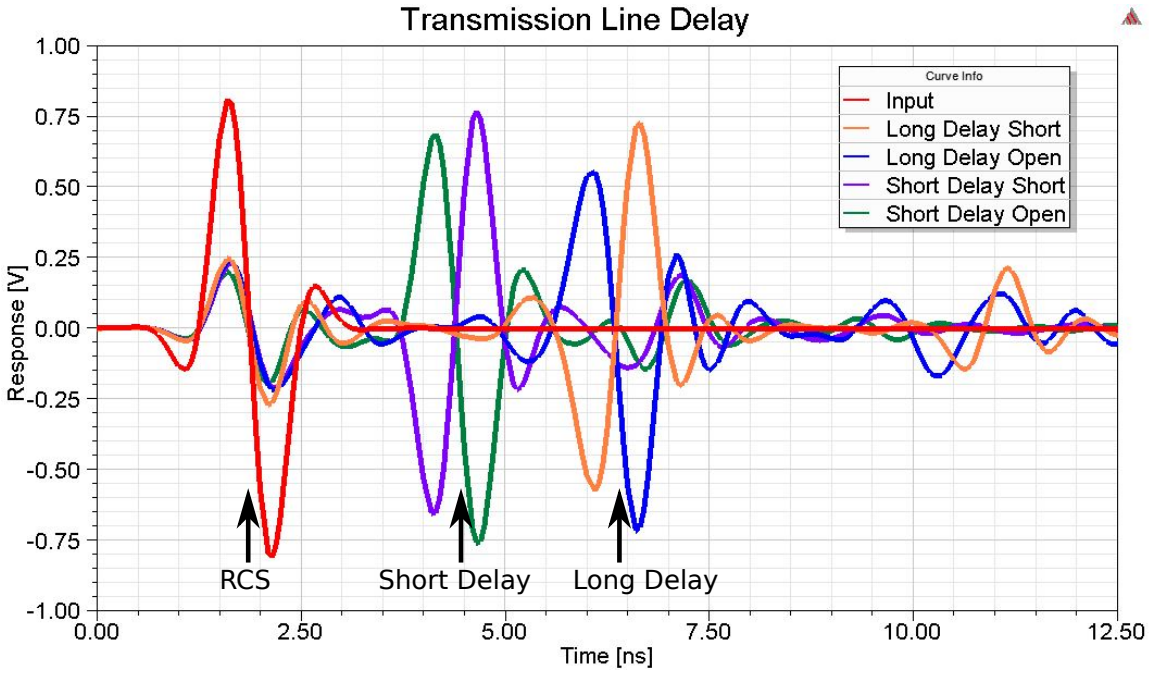

Figure 6.1: Transmission line delay simulation results for Long and Short lines with open and closed circuits at the termination.

6.3 Antenna Simulation

A UWB planar circular antenna was used to produce patterns similar to regular dipoles as shown in Fig. 6.2(a). If in the presence of a dielectric, the antenna will bias

towards the greater dielectric producing either directionality at certain frequencies or lobes as shown in Fig. 6.2(b) and 6.2(c). Since the antenna looks electrically larger, the dielectric lowers the cutoff frequency. For this case, each antenna element has a radius of 50 mm. The reflection parameters for this antenna shown in Fig. 6.3 which, indicates what happens with several different configurations. As expected in free space, the circular planar antenna has a larger bandwidth than dipoles which can be be infinitely thin with a narrow bandwidth. Additionally, when the antenna is directly against a dielectric like PVC, the cutoff frequency decreases more. When next to soil with a larger dielectric constants, the reflection coefficient is increased due to a larger impedance mismatches when referenced to 50Ω.

In the 3D space these antennas can be visualized as in free space and against soil in Fig. 6.4, where the differences can be seen even more. The antennas start out acting like a dipole pattern, but when next to the dielectric their patterns become more directive with an increased number of sidelobes.

This type of simulation can be carried over for bowtie antennas and cloverleaf antennas. Bowtie antennas perform similarly to the planar circular antennas as noted in Fig. 6.5. However, the cloverleaf antenna does not nearly have as much as a definite dipole shape as either of the previous two antennas noted in Fig. 6.6. Instead the main lobe of the antenna is directed in the opposite direction of the feed from the CPW. With the clover leaf antenna, the dielectric half space helps correct the antenna pattern by biasing it more towards the dielectrics direction, which should ideally be towards the surface. However when the bowtie antenna is placed over the dielectric half space, its side lobes increase over either of the previous designs. The more that

is known about the antennas in this type of space, the better the predictions that can be made. If the sidelobes and directional lobes were not pointing towards the surface, there would be a much smaller chance of seeing a response from the antenna as if it might have been a low observable antenna with an extremely low gain and radar cross section.

Based off of these simulations and looking ahead at the requirements for these antennas on buried pipelines, the circular planar antenna design is likely the best balance of response and complexity. Although the bowtie antennas are simpler than the circular antennas, these designs will probably not be able to accommodate long enough transmission lines to create a long enough delay for detection. The similar pattern of the cloverleaf antenna design should perform nearly as well as the regular circular planar antenna. However in the cross polarization configuration, it faces similar problems facing the same limitation as the bowtie antennas, not being able to hold as much transmission line. In the polarization independent case, the cloverleaf design works nearly as well as the circular planar antenna, however the cloverleaf design suffers from challenges associated with having enough physical space on the host structure to allow for stacking. Whereas circular planar antenna can be stacked in series, that is where the driven element acts as the grounding element for the antenna next to it to increase the response along the length of the pipe, cloverleaf antennas have to be separated by at least a diameter's length away. Noting the increased gain from using multiple antenna ports in the cloverleaf design, the basic circular design, depending how large a surface is, can be parallelized, however even with the increased gain, the cloverleaf design suffers from heavy main lobes that do

not directly point towards the potential surface while underground. That having two circular planar antennas that are separated by one diameter's width where the total width equals three diameters over the cloverleaf's two diameter's width. With all of these considered, the moderately simple circular planar antenna is the best antenna candidate.

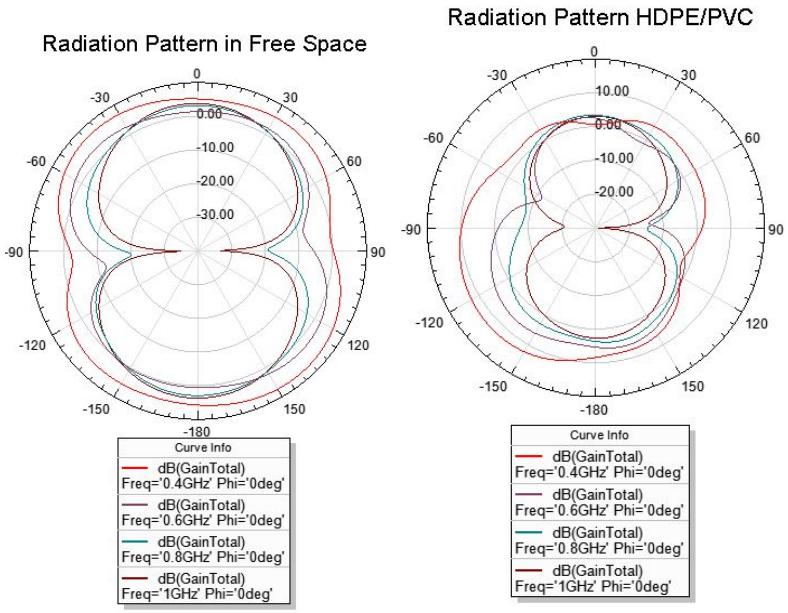

(a)

(b)

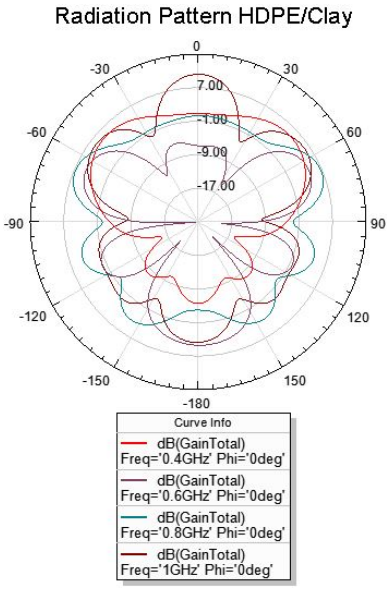

(c)

Figure 6.2: Antenna radiation patterns of Wide-band Planar Circular Antennas at 400, 600, 800 and 1000 MHz varying in (a) free space, (b) between PVC and HDPE, and (c) between HDPE and soil. Note: 0° is in the direction of the dielectric.

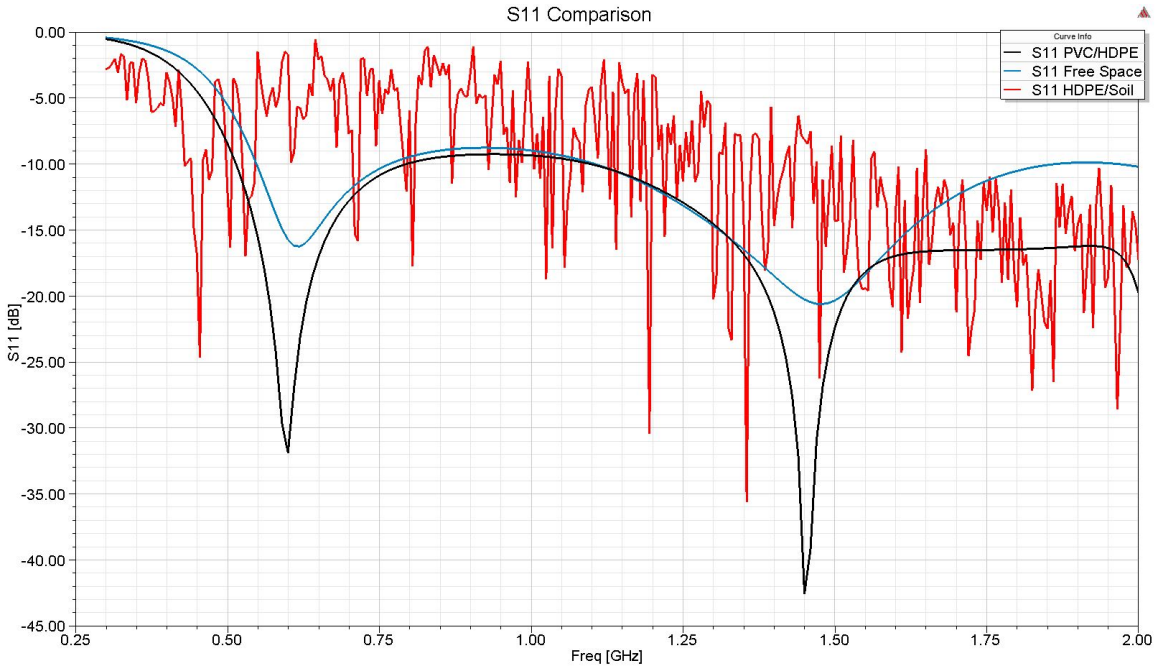

Figure 6.3: S11 comparison between a planar circular antenna in free space, between PVC and HDPE and between HDPE and soil with a dielectric constant of 16.

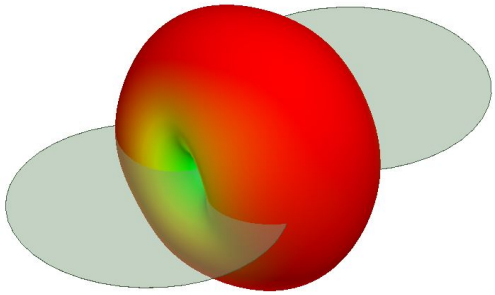

(a)

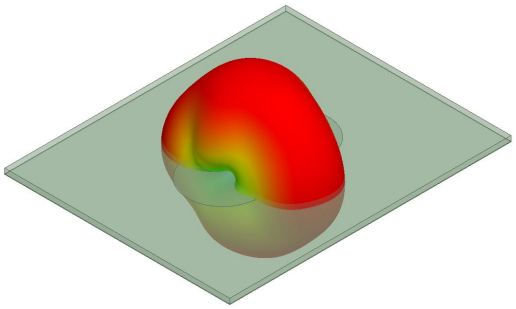

(b)

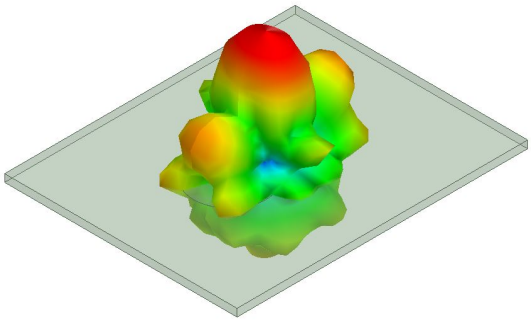

(c)

Figure 6.4: 3D pattern for a planar circular antenna in (a) free space, (b) between PVC and HDPE, and (c) between HDPE and soil at 1 GHz.

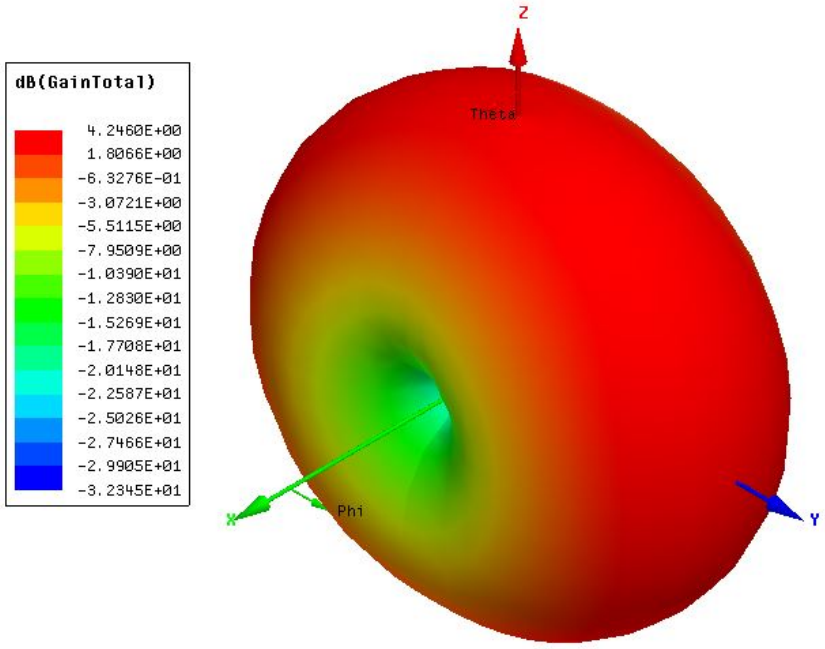

(a)

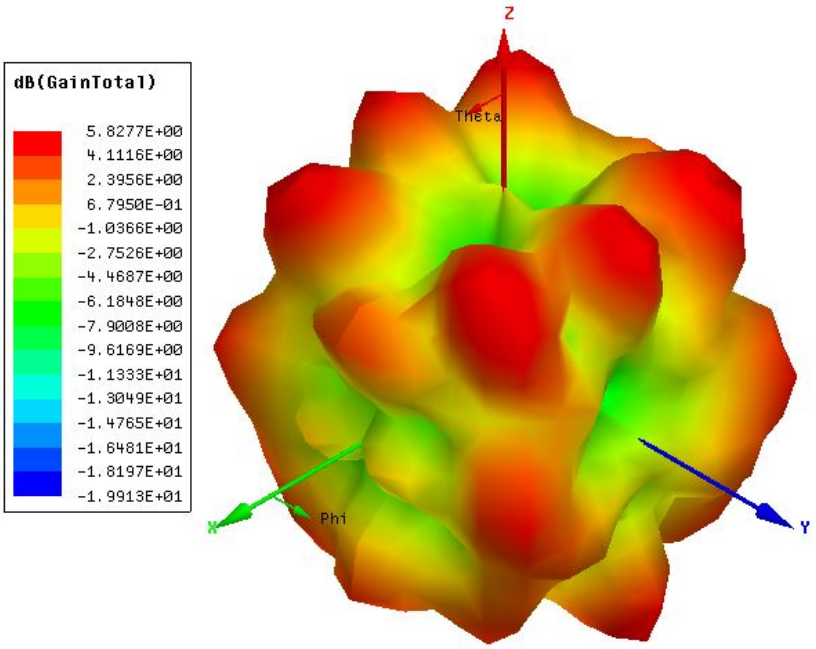

(b)

Figure 6.5: 3D antenna pattern for single port for double bowtie antenna in (a) between PVC and HDPE and (b) between HDPE and soil at 1 GHz.

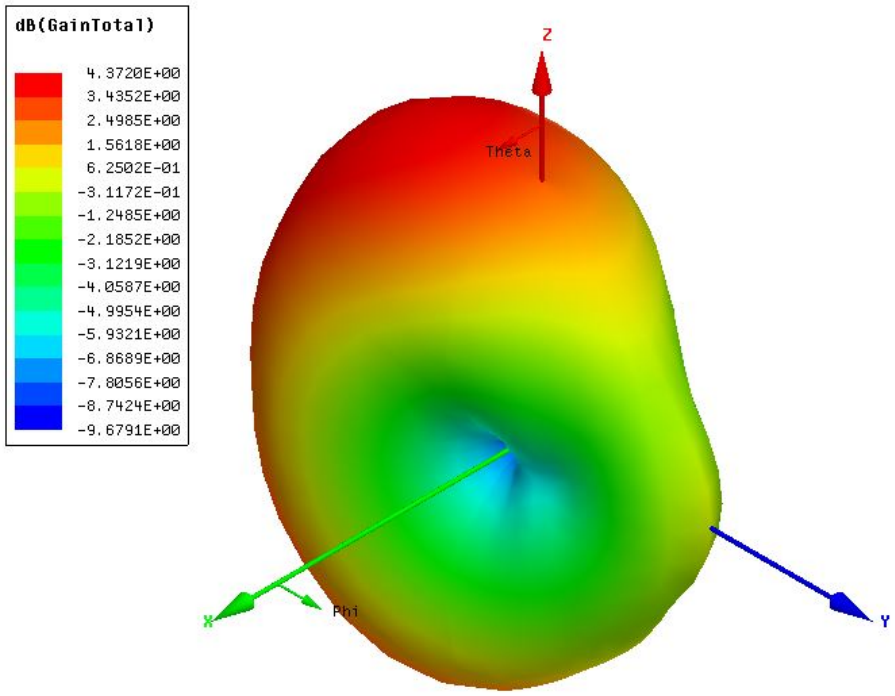

(a)

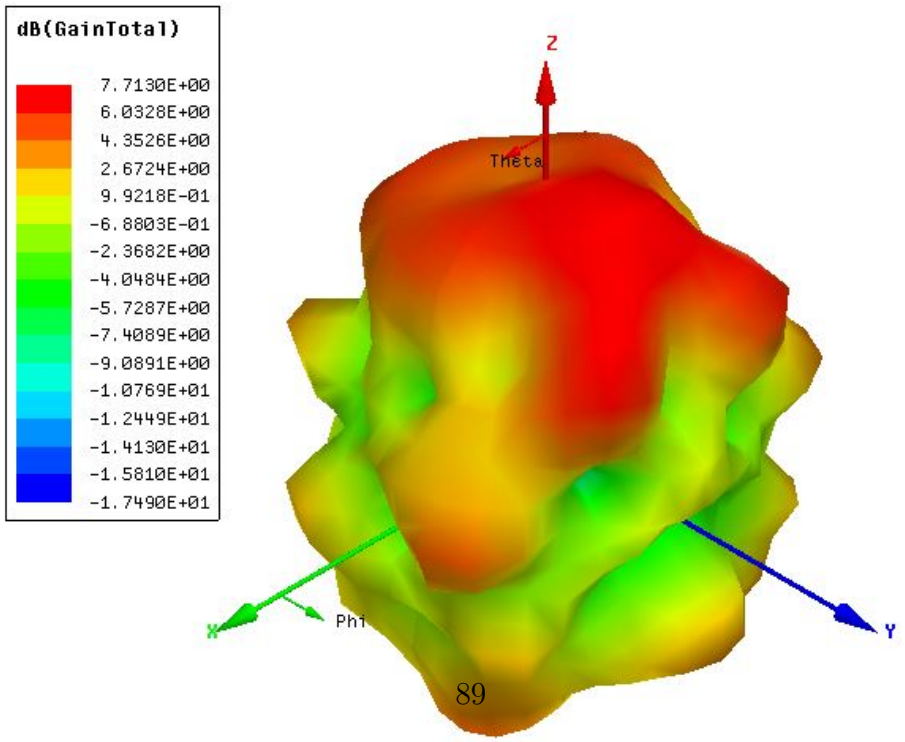

(b)

Figure 6.6: 3D antenna pattern for single port for cloverleaf antenna in (a) between PVC and HDPE and (b) between HDPE and soil at 1 GHz.

Chapter 7

Delay Line Tags Simulation

The overall approach of coplanar tags is displayed in Fig. 7.1, which starts with UWB antenna that combined is with varying lengths of CPW to create a delay line tag. If a polarization independent tag is needed, then the simple delay line tag is duplicated and rotated four times. The same concept is applied with cross polarization tags, but instead it uses two antennas connected or by transmission lines changing the polarization. If a transmission line is used in a cross polarization tag the transmission line can delay the incident pulse too.

7.0.1 Co-polarization Tag

When scanning with a GPR, that is over multiple A-scans, these simple delay line tags produce responses that look like two hyperbolas. As Dardari noted earlier, one is produced by the radar cross section of the tag and the other is from transmission of the delay line of the tag as seen in Fig. 7.2(a) [22]. Although the transmission line

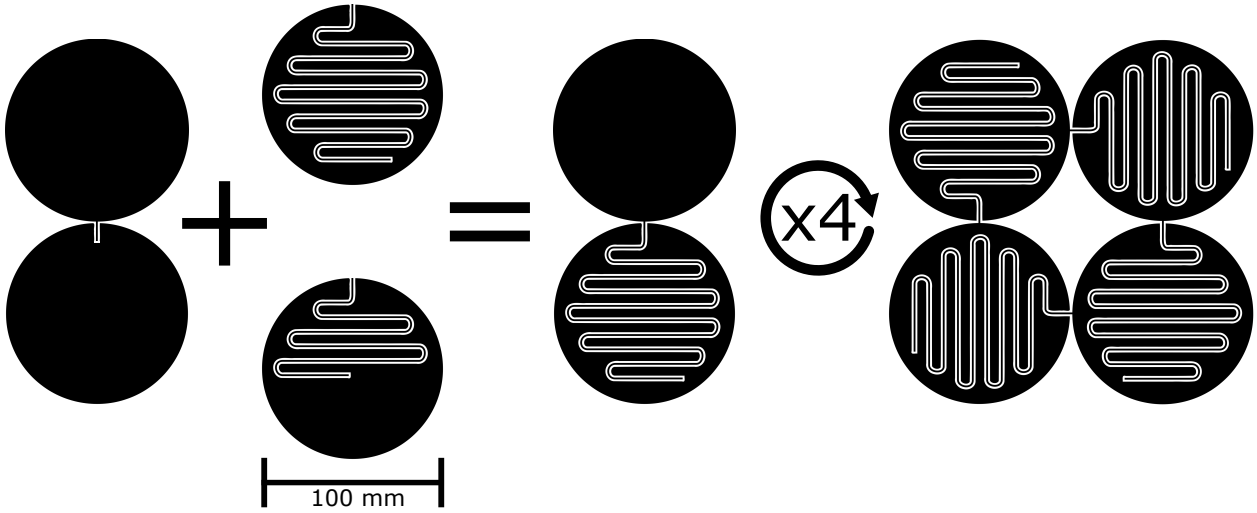

Figure 7.1: Wide-band planar circular antenna using two aluminum circles with a radius of 50 mm fed through a CPW with a width of 1 mm and a gap of 0.5 mm. This is then connected to a transmission line delay with a physical length of 369 mm or 660 mm terminated with an open circuit. When combined, the antenna and transmission line creates the transmission line delay tag. Similarly a polarization independent transmission line delay tag is created by turning and quadrupling the transmission lines by 90°.

simulations show clear differences between the open and closed circuit delay lines in Fig. 6.1, when the antenna and transmission line are combined, the shunted delay line tags do not reflect nearly as well as the open delay line tags as shown in the B-scans of Fig. 7.2(a) and 7.2(b).

This type of tag has been simulated with soil conditions, where the tag is placed on top of sudo rectangular 4-inch HDPE pipe such as the one illustrated in Fig. 7.3. This was done to decrease the simulation time and memory usage in HFSS, where otherwise the simulation might crash. The delayed line hyperbola can be discerned from the large response from the change in dielectrics in Fig. 7.2(e) with a long open delayed line. These results verify the claims that delayed line tags, similar to this, produce a second response. This antenna response, not having been investigated through the lens of a GPR, would look like a second hyperbola.

7.0.2 Polarization Independent Tag

Using the same delay transmission lines from the last section, the simple delay line tags can be duplicated and rotated around a central axis, producing a polarization independent tag operating both in horizontal and vertical polarizations. Fig. 7.4 demonstrates this concept in operation by comparing two incident waves with perpendicular polarizations reflecting off of a simple delay line tag and the polarization independent tag, both with the same delay. Although the simple delay line tag produces structural mode scattering, it does not produce any antenna mode scattering with the perpendicularly polarized incident wave. Contrasting with the polarization independent tag, this tag works with both incident pulses with the exact same response.

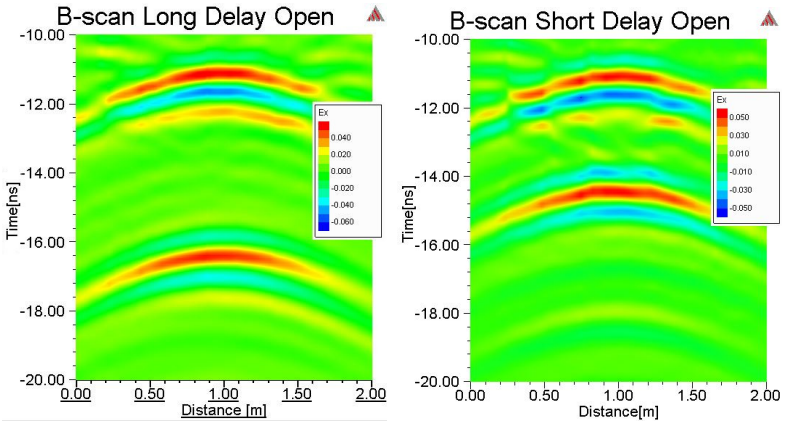

Figure 7.2: B-scans from a (a) long open delay line tag, (b) short open delay line tag,(c) long closed delay line tag, (d) short closed delay line tag, (e) long open delay line tag in dielectric environment on top of a simulated HDPE pipe. The legend is an indication of the electric field received one meter away from the tag after an incident plane wave pulse. For (e), the legend's max and min have been reduced in order to see the second response from the tag at 35 ns over the response from the rectangular pipe at both 20 and 25 ns.

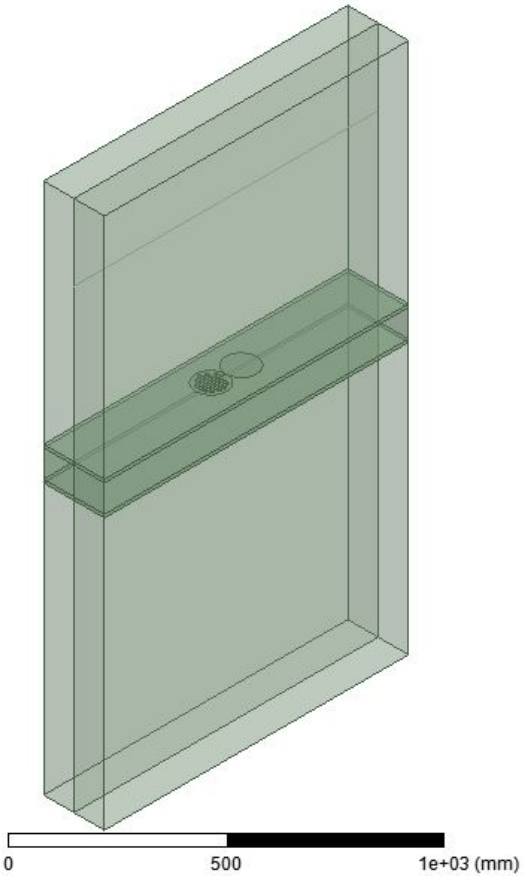

Figure 7.3: Model of long open delay line tag in soil with a dielectric constant of 16 and a conductivity of 0.001 S/m placed on top of an equivalent rectangular 4-inch HDPE pipe.

This tag design is simpler than the more complicated circular polarized delay line tags that are used in Shen [56]. These tags would work well with the "Yakumo" multi-static GPR, from Sato, that measures the vertical and horizontal pulse responses, doubly confirming that a tag exists over natural objects [54]. This tag minimizes the chance of user error, if a GPR is run over a single polarization.

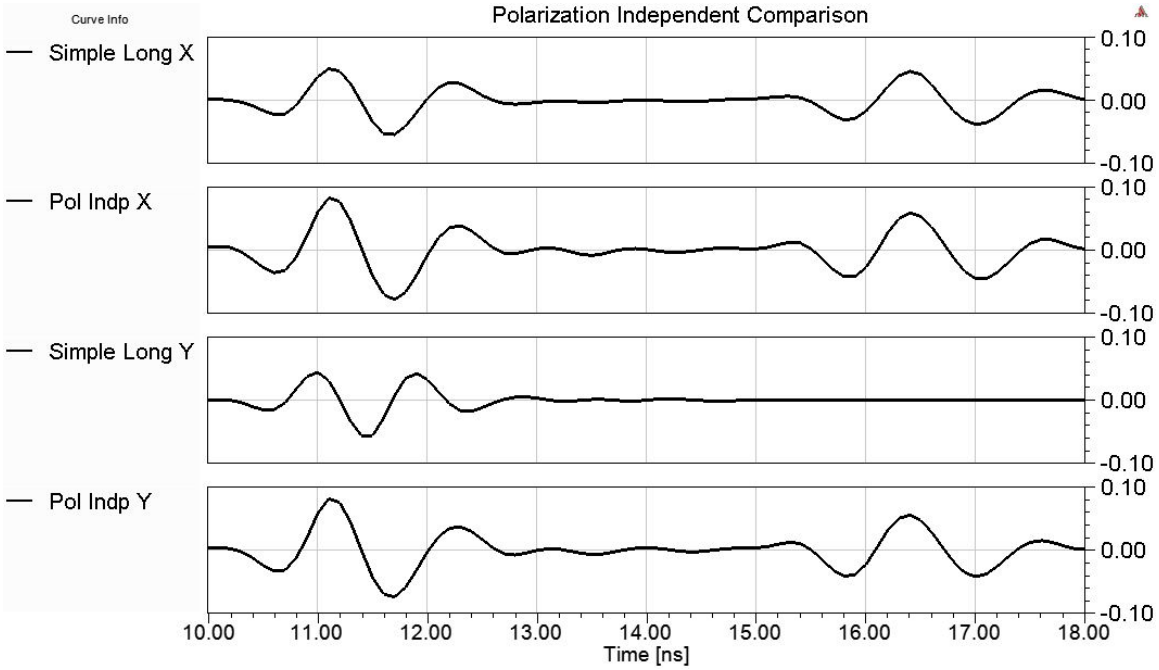

Figure 7.4: A-scan simulation comparing polarization independent delay line tags and simple delay line tags while changing the incident wave's polarization where the X axis is the collinear polarization response and the Y axis is the cross polarization response.

7.1 Cross Polarization Delay Line Tag

Cross polarization tags can only differentiate between a short delayed signal and a long delayed signal. Similar to Feng, two bow tie antennas can be combined perpendicularly [26]. Using the tags from Fig. 7.5(a), 7.5(b), and 7.5(c), Fig. 7.7 compares the responses from the CP tags and the simple delay line tags similar to that of the polarimetric GPR. The simple delay line tag responds in the horizontal polarization, however all three of the CP tags respond in the vertical polarization with varying delays. Because the bowtie CP tag is directly coupled, it has the shortest delay of 0.5 ns, followed by the short CP tag with a delay of 1 ns and the long CP tag with a delay of 2.5 ns. If these were in other dielectric environments, as discussed earlier, these tags would have longer delays. The bowtie CP tag has a smaller response than the other two CP tags mainly because it uses one antenna pair instead of two antenna pairs like the other two tags. If two of these bowtie tags were used in parallel, the size of the response should be much more like the other CP tags. In general, the simulations for these CP tags are promising, because of their greater perpendicular response not nearly as noticed by ordinary targets.

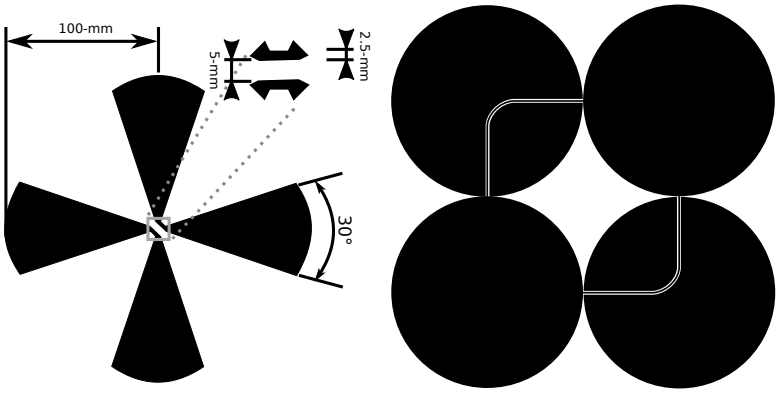

(a) (b)

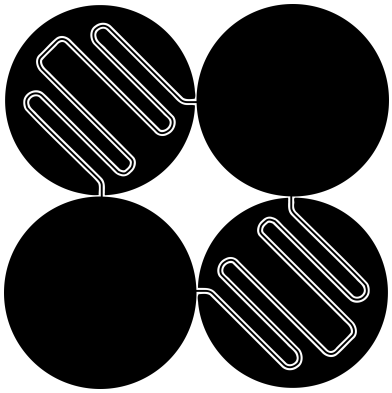

(c)

Figure 7.5: (a) Simple cross polarization tag with two bowtie antennas with an overall length of 200 mm and angles of 30° (b) double cross polarization tag with a physical transmission line length of 98 mm (c) double cross polarization tag with a physical transmission line length of 332 mm.

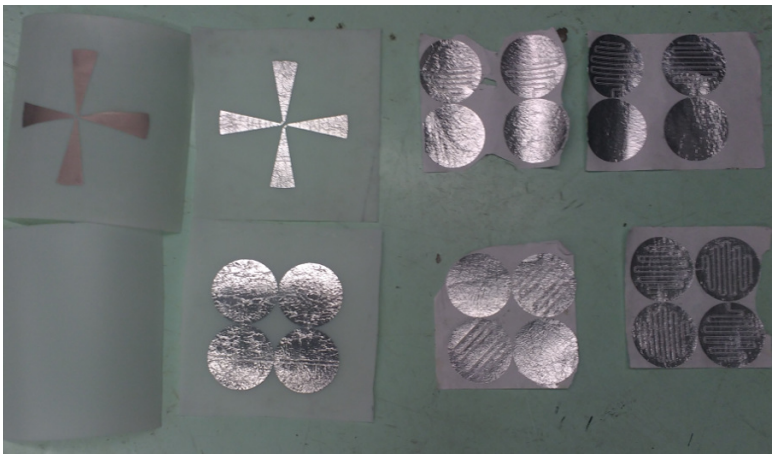

Figure 7.6: Manufactured tags from top to bottom left to right: Spray paint cross polarized bowtie, HDPE blank, Aluminum foil cross polarized bowtie, short cross polarized tag, short linear polarized simple tag, long cross polarized tag, long linear polarized simple tag, long polarization independent tag.

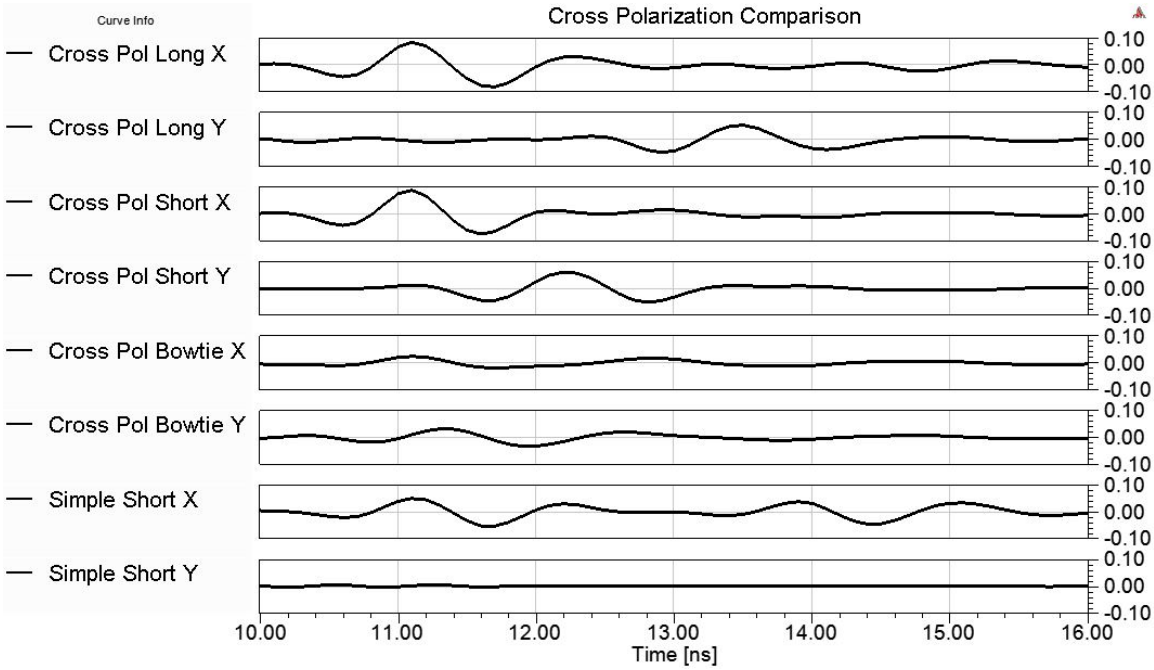

Figure 7.7: A-scan simulation results with results from recording the X and Y polarizations from simple delay line tags and cross polarization tags where the X axis is the collinear polarization response and the Y axis is the cross polarization response.

Chapter 8

Tag Characterization - Experimental Methods

The simulations and manufactured tags need to then be tested in a controlled environment. These tests start with some simple antenna measurements and then move on to day in the life tests.

8.1 Antenna Measurements

As discussed earlier, the antennas will be adversely detuned when the bulk dielectric constant around the antenna under test (DUT). The tests for a simple dipole wire antenna, with quarter wavelength elements equal to 60 mm as shown in Fig. 8.1, should indicate center frequency shifts and antenna pattern biasing with varying dielectric half spaces. Setup for S11 and antenna gain measurements in dielectric half spaces is recorded below.

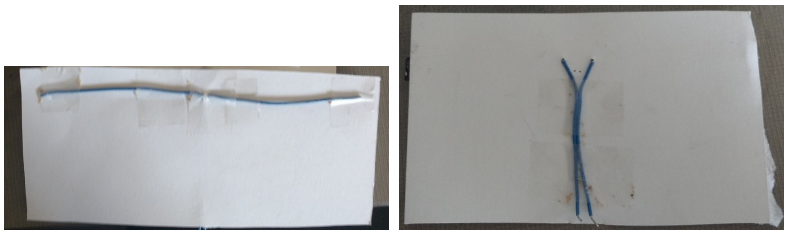

(a) (b)

Figure 8.1: Dipole antenna with elements 60 mm long on a 3-in by 5-in note card in the (a) front and (b) back.

8.1.1 Reflection Parameters of Antennas

To see reflection parameters or S11 of antennas in varying conditions, a HP8753C vector network analyzer (VNA) measures S11 characteristics of antennas mounted to varying materials. The pictures below in Fig. 8.2 show three cases, outside of free space measurements, that change the S11 parameters. The primary factor changing the S11 parameters in these tests is the dielectric constant which will change the electrical shape of any antenna as opposed to the physical shape of the antenna which remains the same. Take for example the dipole: what might have been half a wavelength long at one frequency might be something like three quarters of a wavelength when in a dielectric half space. The dielectric half space detunes the antenna to a lower frequency. With varying dielectric half space environments, one can then predict how other environments will affect AUT. The structure and material of the half spaces affects how the S11 parameters and impedances change. If the antenna is not directly coupled (like the TiO_2 powder that is separated by a lower dielectric paper bag), the S11 parameters will not change as much. The frequency sweep from the VNA uses a HPIB to USB converter and the KE5FX VNA Utility

software to produce a file using real and imaginary numbers as displayed in Fig. 8.3.

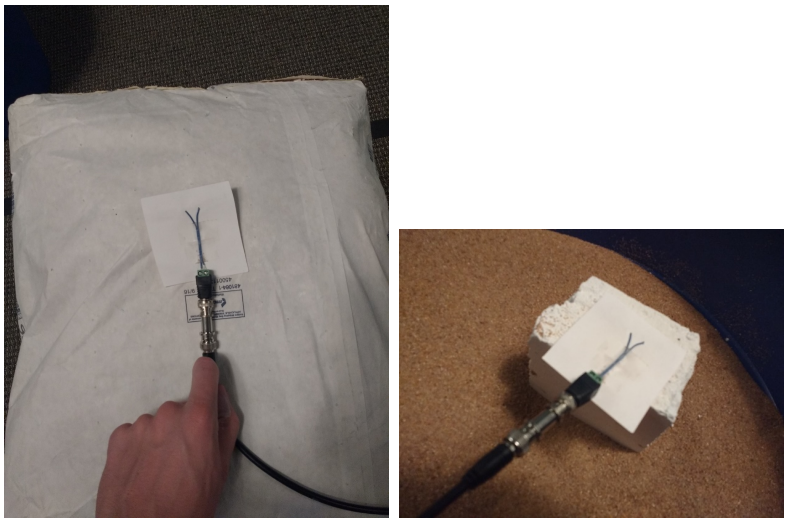

(a) (b)

(c)

Figure 8.2: S11 antenna measurements when (a) on top of a TiO_2 bag, (b) TiO_2 block and (c) sand.

8.1.2 Antenna Range

Antenna gain measurements can range from highly accurate testing in anechoic chambers filled with absorbing materials and a mechanized rig to having two antennas in the middle of an open field and changing the angle of the AUT manually. This

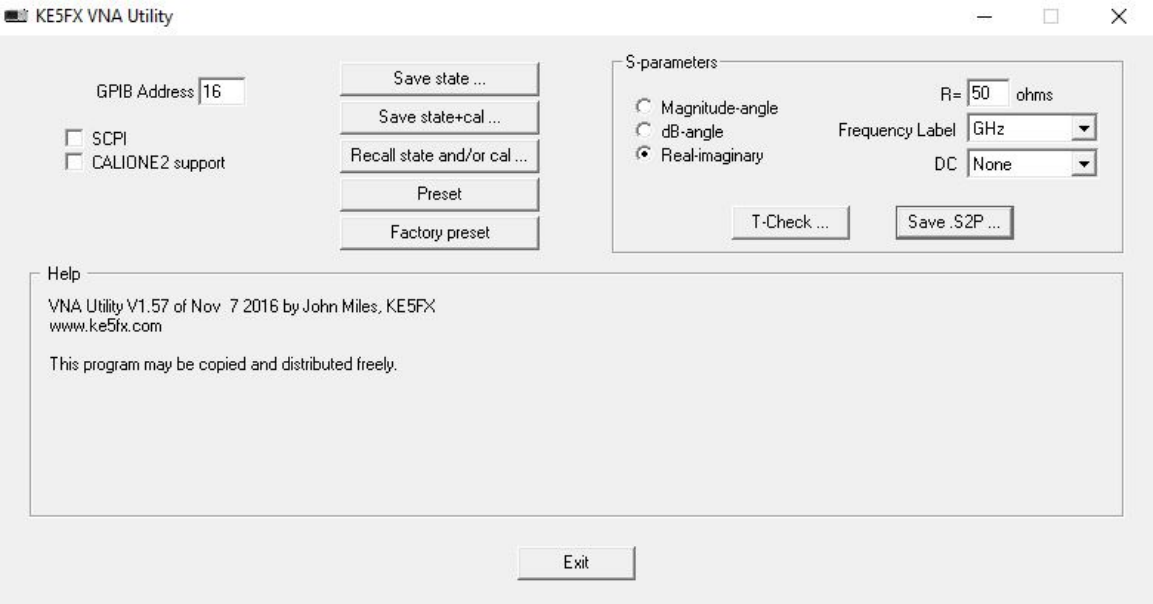

Figure 8.3: KE5FX VNA Utility Program running on Windows 10.

thesis documents the latter case. To obtain accurate results, minimizing multipath propagation, a spot in the middle of an open room is chosen that is about ten wavelengths of the desired frequency from any other large objects like in Fig. 8.4. A directional reference antenna is also placed about the same distance away pointing towards the AUT with Fig. 8.5. A signal is transmitted on the reference antenna with a signal generator and the power is received on the AUT with equipment in Fig. 8.6. To verify the angle, a compass is used for the AUT. To simulate half dielectric spaces, a TiO_2 and gypsum block with an approximate dielectric constant of 16 is placed in front of AUTs like in Fig. 8.7.

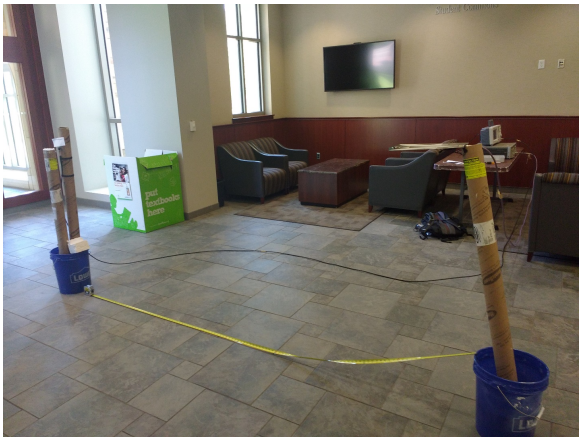

Figure 8.4: Indoor antenna range in Rayzor Hall lobby.

8.2 Free Space Tests

A free space test verifies the viability of potential tag candidates before testing them underground. To do this, the VNA frequency sweeps from 800 MHz to 6 GHz with two RF Space TSA600 Vivaldi Antennas to create a bi-static radar that are separated by at least half a wavelength from the lowest frequency or 0.188 m. This is similar to a study done in the late 1980's by Thain when using an older VNA for detecting pipes [58]. The bottom of both antennas are 10 cm away from the ground. For the cross polarization case, the set of two antennas offset each other by 90° and are also separated by the same distance. The tags are then placed in the middle of a 1-foot long 4-in diameter PVC pipe. The file from the VNA is then imported to AWR Microwave Office and transformed into time domain reflectometry (TDR) results producing an A-scan. The time resolution for this transformation is set to the limit of 128 and the window used is a Hanning filter. The windows are used in order to better simulate a pulse in the time domain. These results in the time domain are

Figure 8.5: Reference Vivaldi antenna on cardboard tube.

then exported in a .csv and then transferred to a Python script that either produces stacked plots of A-scans or B-scans. These B-scans are plotted with A-scans over a change of distance. The code for the B-scan plotting originally came from gprMax which is an open source GPR simulation software [62]. The python code for these is in the first appendix. In this case, the change of distance between each A-scan is 12.5 cm. Although these tags will ultimately be on top of HDPE pipes, these PVC pipes produces a good enough approximations. The pipe, with the tags in them are

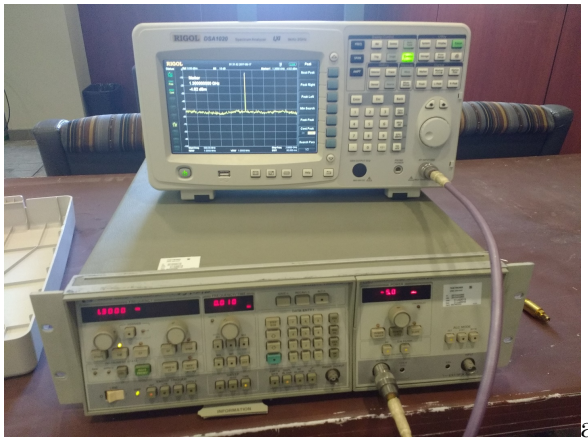

antennas under testing

Figure 8.6: Signal Generator and Spectrum Analyzer for AUT.

placed 2m in front of the bi-static setup shown in Fig. 8.8.

8.2.1 Underground Tests

After the free space tests, the tags need to be tested in an in-situ environment similar to its intended use case. However this does not mean a tag has to be directly on top of a pipe and buried underground every single time. In line with the previous free space tests, quick underground tests are proposed.

Instead of having the tags placed on top of the intended pipes, they are instead placed inside of an underground pipe to quickly move any needed tag into place. The underground pipe can be accessed through 90° connections to the top of the soil. Irrigation valve boxes cover up the pipes to reduce water infiltration and any safety hazards of falling into the hole. In this case, the length of the straight pipe is 8-feet and the top of the pipe is 0.36 m from the surface just noted in Fig. 8.9. In order to move the tag through the underground pipe, cables are placed before hand,

Figure 8.7: AUT test setup with TiO_2 block.

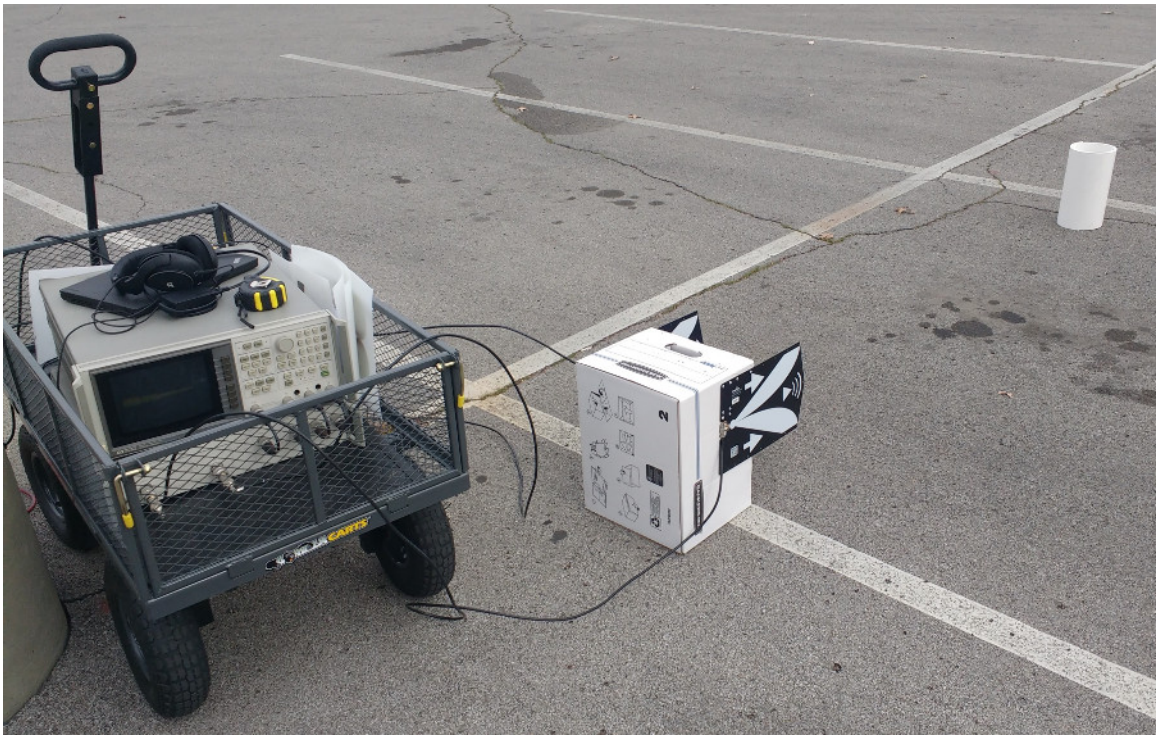

Figure 8.8: Outside test setup in the middle of a parking lot with a co polarization setup.

where a HDPE carrier sheet can move the tags into place as described in Fig. 8.10.

Figure 8.9: 8-foot long underground pipe before soil is placed on top.

The GPR used for the underground tests of the tags is the GSSI-SIR-3000 using a 200 MHz and 400 MHz antenna. The 200 MHz antenna, Model 5106/A, is dragged along the ground while the 400 MHz antenna, Model 50400S, is carried over the target with a cart, Model 62X. Both antennas connect to odometers that trigger

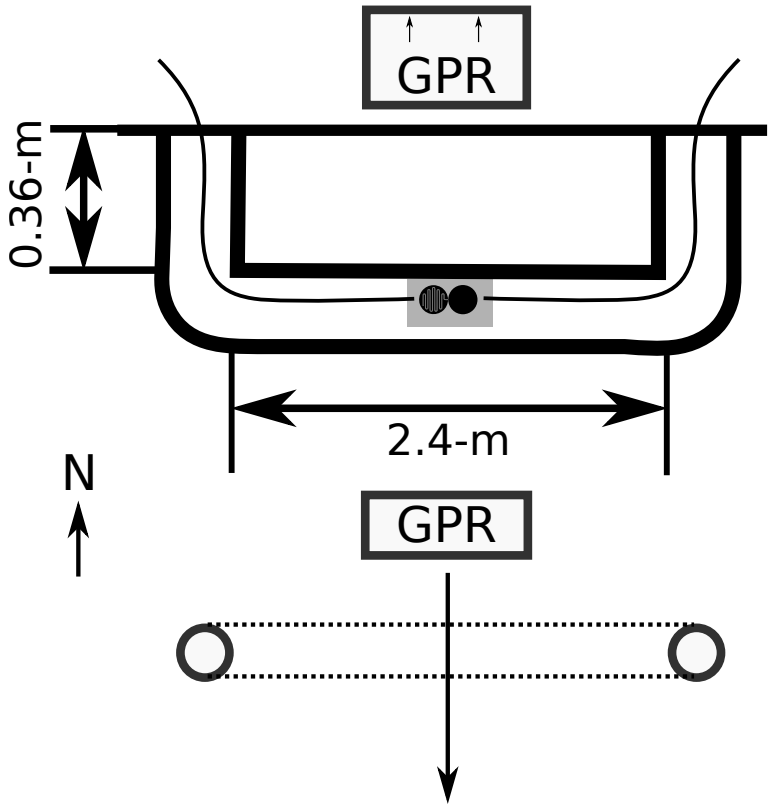

Figure 8.10: Underground pipe setup that includes a common HDPE carrier connected to a fishing line to go through the pipe. The bottom half of this setup diagram indicates how the GPR is moved over the sample and pipe including cardinal directions.

GPR pulses after the wheel has gone a certain distance. In this case the wheel is behind and in front of the antenna respectively. Before carrying out the tests, the odometer needs to be calibrated. To do this, a known distance, measured with a measuring tape, is set and to start the calibration run go under the COLLECT menu, under RADAR, under MODE and select distance, where it will give instructions on how to proceed. To make sure the SIR-3000 knows the correct antenna used, go

under the COLLECT menu and under RADAR select the antenna frequency used. The full menu is displayed in Fig. 8.11, where more details can be found in the GSSI-SIR-3000 manual. To start or stop collection of data, press RUN/STOP and to start a single B-scan, press RUN/SETUP. When it beeps twice after that, proceed with the B-scan where to end it, press RUN/SETUP again and select the file name for the B-scan. To transfer the B-scan files to the computer, connect a USB into the port and select OUTPUT to the TRANSFER submenu and select HD. After that, check which files to transfer and press the right key. These files may then be post processed with either GSSI's RADAN software or GP Workbench.

Specific tags can be tested with varying degrees of polarization mismatch. Linearly polarized simple delay line tags have to first be tested with 0° of mismatch. Then when testing against the polarization independent tags will need to be tested with 45° and 90° of mismatch. The polarization independent tags only need to be tested with 0° and 45° of mismatch, since these tags will have the same response when rotated 90°. Cross polarization tags will need to have approximately 45° of mismatch in order to work with the co-polarized GPR.

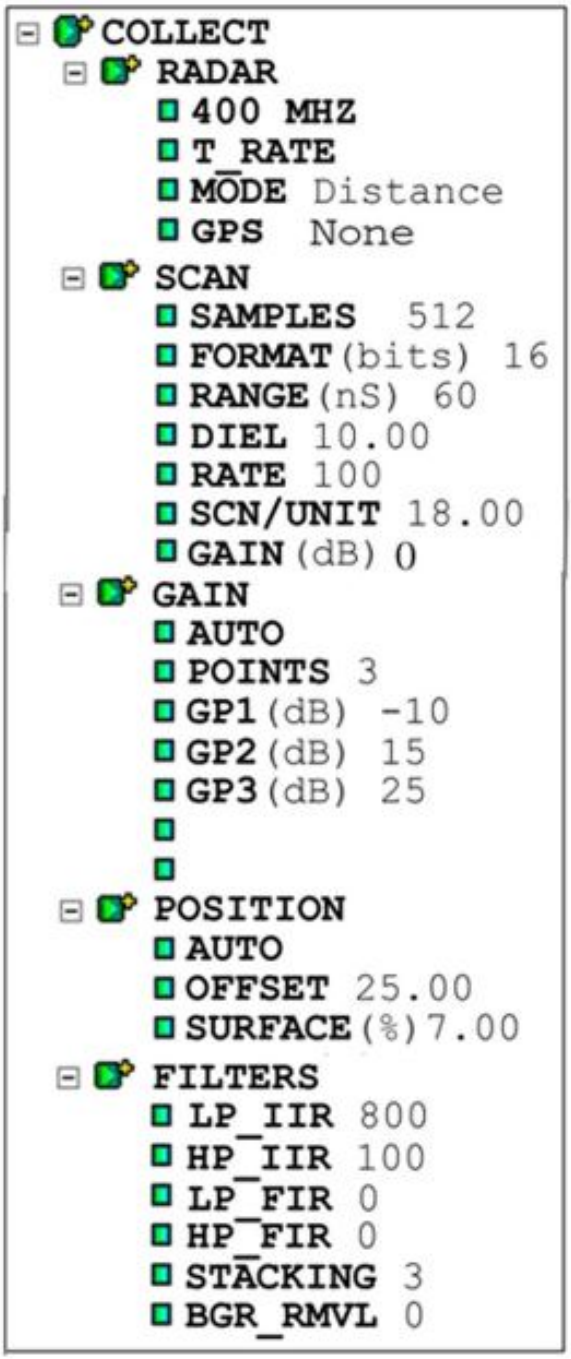

Figure 8.11: Full SIR-3000 Menu

Chapter 9

Characterization of Tags

Using the testbeds described in Chapter 4, the results are interpreted with basic antenna measurements, free space tests and underground GPR tag tests. The basic antenna tests, simply verifies how dielectric environments change antenna parameters. The free space and underground tests use the tags manufactured with the Silhouette Cameo from Chapter 3.

9.1 Antenna Measurements

As expected, when a dipole is in the presence of a dielectric half space, it detunes to a lower frequency. In this case, in free space it was tuned to about 1 GHz. As for the reflection parameters, the antenna, when in the presence of a TiO_2 bag, is barely detuned since it is more coupled to the paper and air than the TiO_2 and for all intents and purposes resonates at the same frequency as the free space test. When in a sand half space, the dipole resonates instead at 900 MHz and when in the TiO_2

half space, it resonates lower at 850 MHz as noted in Fig. 9.1. Although the sand has a lower dielectric constant, it conforms to the dipole antenna more than the TiO_2 block thus increasing the coupling between the sand.

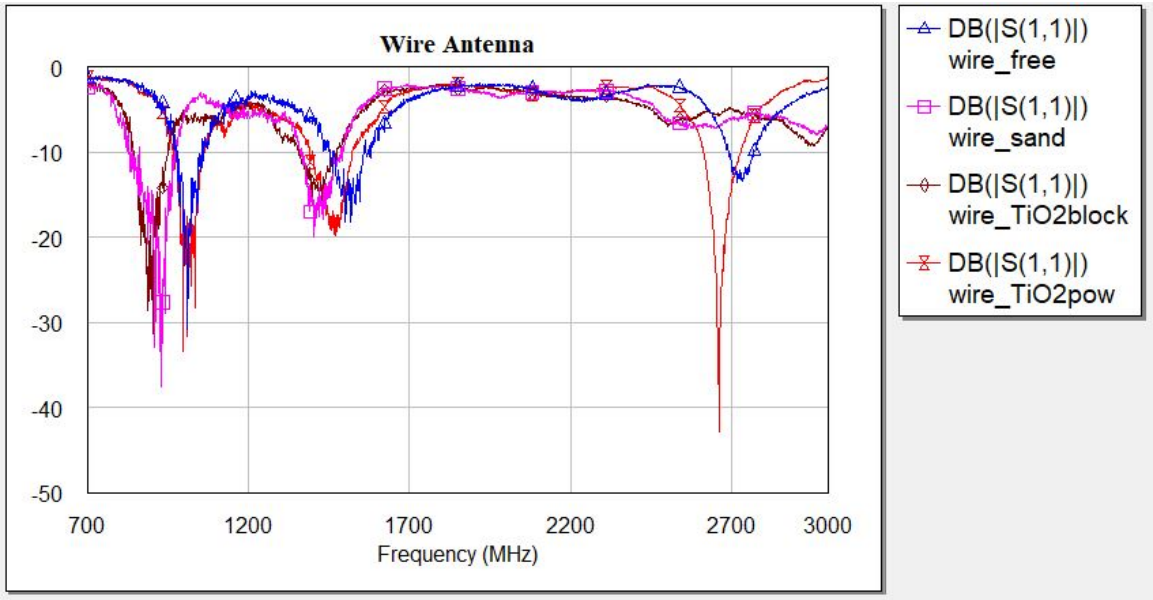

Figure 9.1: S11 parameters for simple dipole in free space, against sand, against TiO_2 powder and against TiO_2/Gypsum block.

Although 3D measurements of antenna gains can not be taken with current equipment, 2D equivalents work, when changing either the phi or theta angles that is when measuring with respect to vertical and horizontal polarizations. As expected in free space measuring across the horizontal polarization, nulls can be seen at 90° and a fairly constant gain can be seen when measuring across the vertical polarization. However, when the wire is against the any dielectric, it becomes more directional. The front lobe of the antenna, that is towards the TiO_2 block, has approximately 5 dB greater gain than the free space test. This is further enforced by the nulls with both

horizontal and vertical measurements between 90° and 120°. These measurements verify the simulations showing how half spaces change antenna patterns from Fig. 6.2.

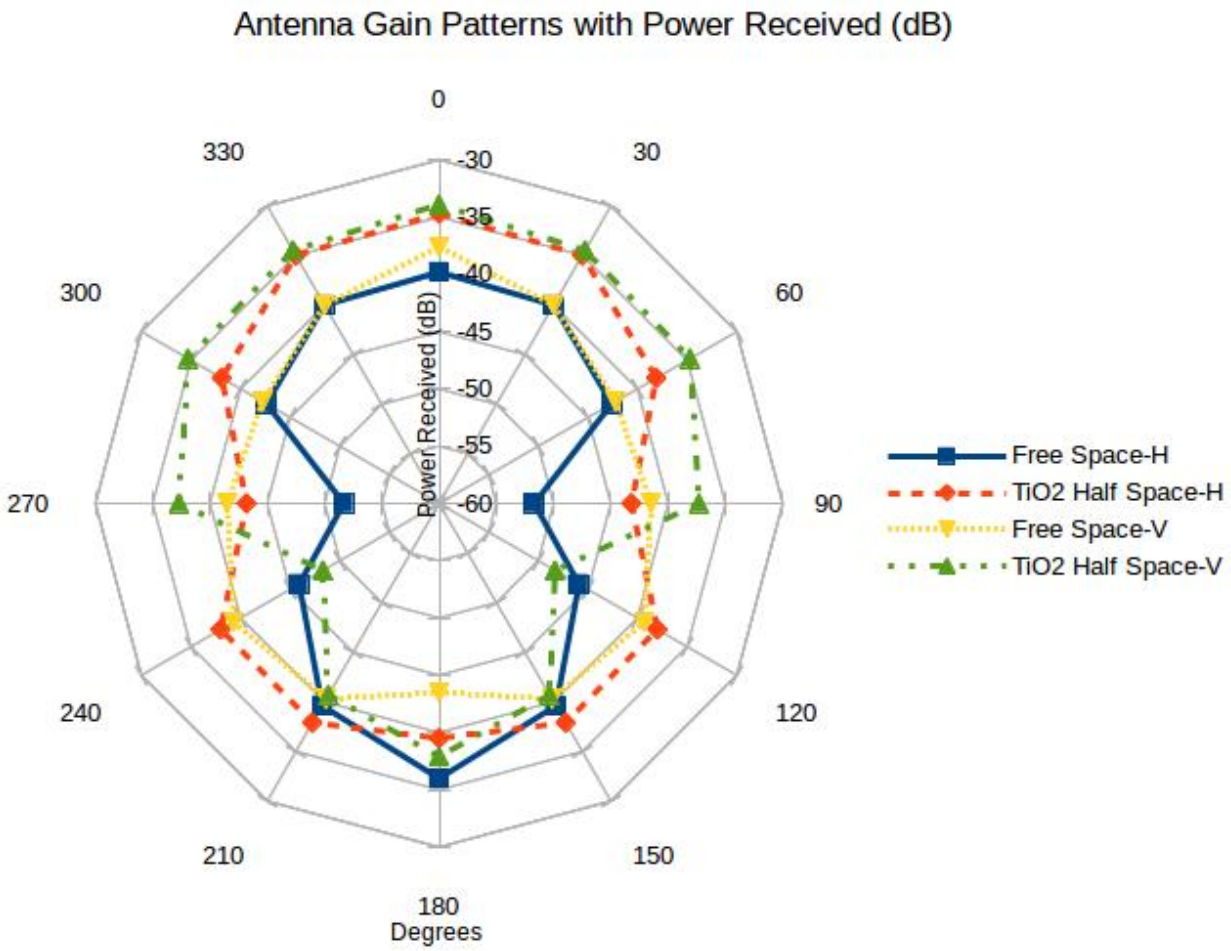

Figure 9.2: Antenna gain measurements when wire antenna is in free space and against TiO_2/Gypsum block with horizontal polarized measurements, noted by the h notation and by measuring across angle theta when phi = 0, and vertically polarized measurements, noted by the v notation and by measuring across angle phi when theta = 0. These measurements in reality were only taken from 0° to 180° as noted by Table 9.1.

Table 9.1: Measured received power(dB) to plot antenna gain for Fig. 9.2.

	Horizontal	Polarization	Vertical	Polarization
Degrees	Free Space	TiO_2 Half Space	Free Space	TiO_2 Half Space
0°	-39.8	-34.7	-37.6	-33.9
30°	-40	-35	-40	-34.5
60°	-42.6	-38.1	-42.2	-34.7
90°	-51.7	-43.2	-41.5	-37.3
120°	-45.9	-38	-39.3	-48.3
150°	-39.6	-37.9	-40.3	-40.7
180°	-36	-39.5	-43.5	-37.9

9.2 Above Ground Tag Tests

To then test how the tags function, above ground tests are verified with A-scan results. Fig. 9.3 shows three different A-scans in free space with a control, a plain pipe, and a simple linear polarized tag. Although the initial reflection from the pipe outweighs the secondary response from the tag, like in Fig. 9.4, the response is still present several nanoseconds later. If the tags are rotated 90° such that the polarizations between the tag and antenna mismatch, there is almost no response which is compared to the polarization independent tag which has practically the same response as the long simple delay line tags when properly polarized. Although the CP tags are placed in front of the radar, they should not have a secondary response unless the tag is rotated by 45°. Accounting for polarization mismatch, these CP tags should be able to be seen, however, because their delay is much shorter compared to the simple delay line tags, the response is masked by the structural scattering. For the co-polar case 11 compiled A-scans, to form a B-scan in Fig. 9.5, show the difficulty in discerning the secondary antenna mode response from the polarization

independent tag which should be seen at approximately 22 to 23 ns.

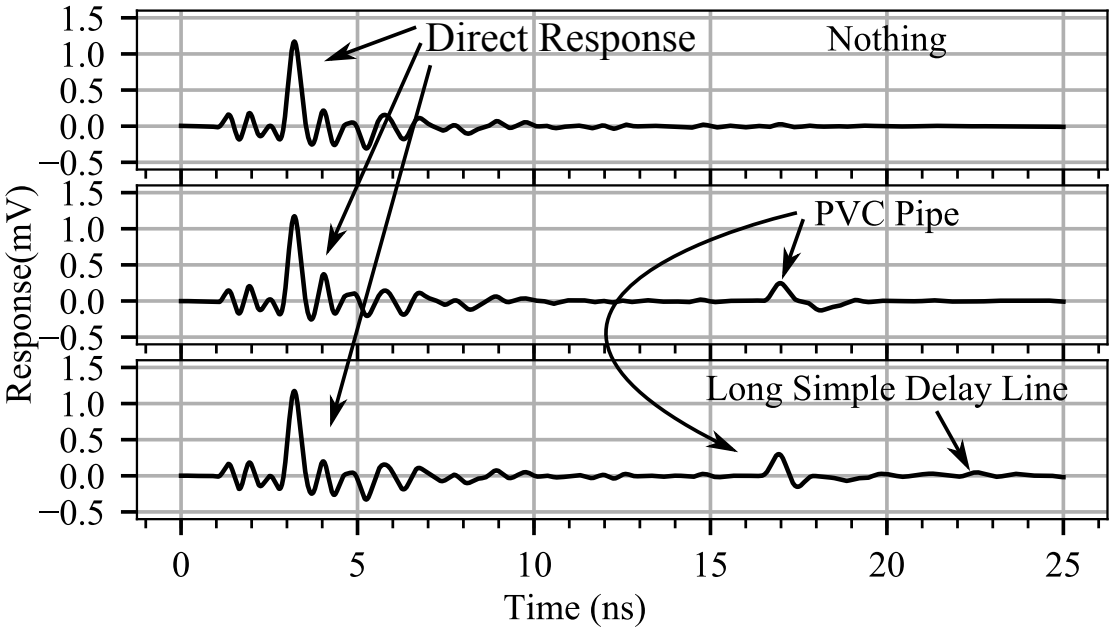

Figure 9.3: Baseline from 0 to 25 ns with antennas in the co-polarization position where "Nothing" represents the free space control test without anything in front of the antennas.

To set up a baseline for the cross polarization test, Fig. 9.6 shows A-scans from nothing, a PVC pipe and a long CP tag from 0 to 25 ns. Although there should be more isolation, the VNA still picks up some near field direct transmissions from the transmitting antenna to the receiving antenna at 4 ns, however this response does not affect the rest of the results since this is early in the A-scan instead of later when the pulse is reflected off the pipe. The structural scattering mode is reduced when in the cross polarized configuration using appropriate CP tags as shown in Fig. 9.7. The polarization independent tags, also tested with the cross polarized and co-polarized case, indicate that there is still a small response, where the response is

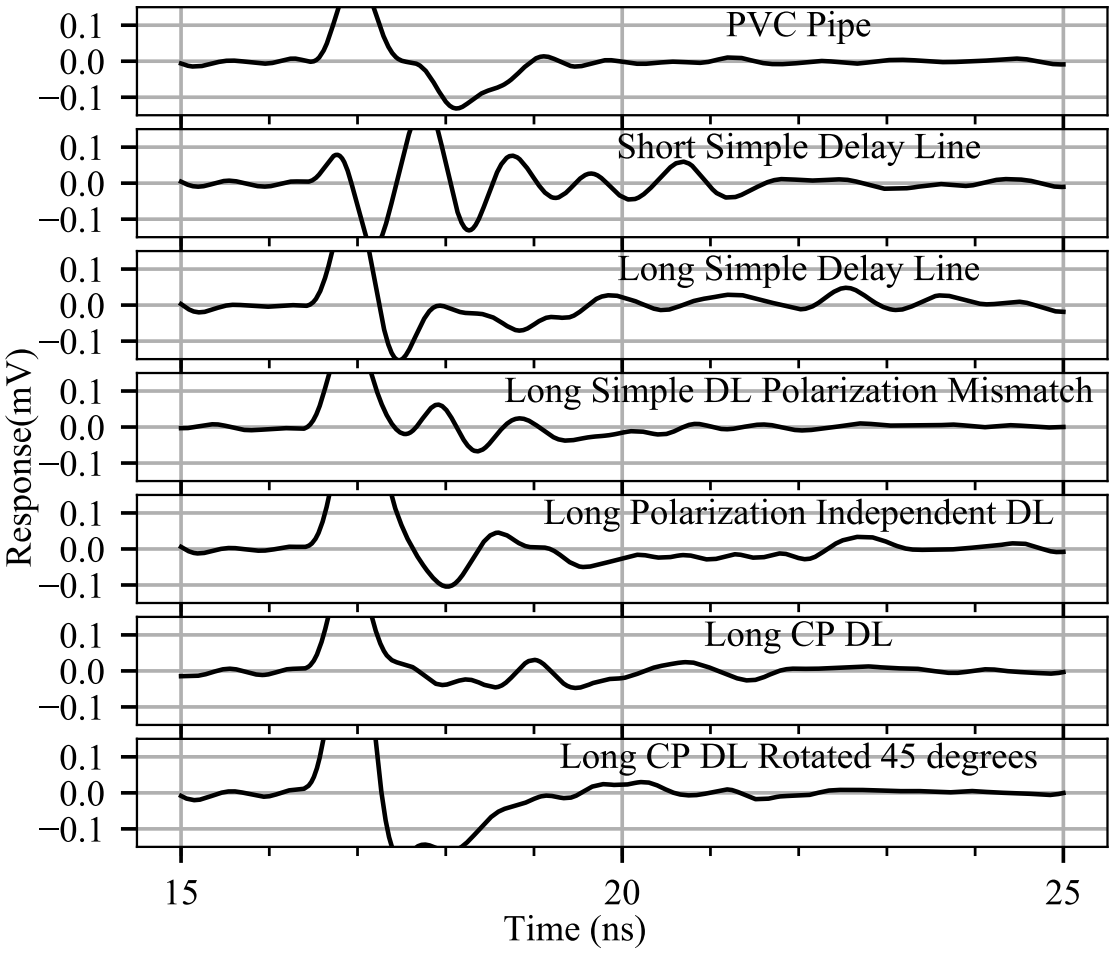

Figure 9.4: A-scans from 15 to 25 ns with antennas in the co-polarization position. Accordingly these A-scans include some of the same A-scans from Fig. 9.3 that are zoomed in to reveal more detail.

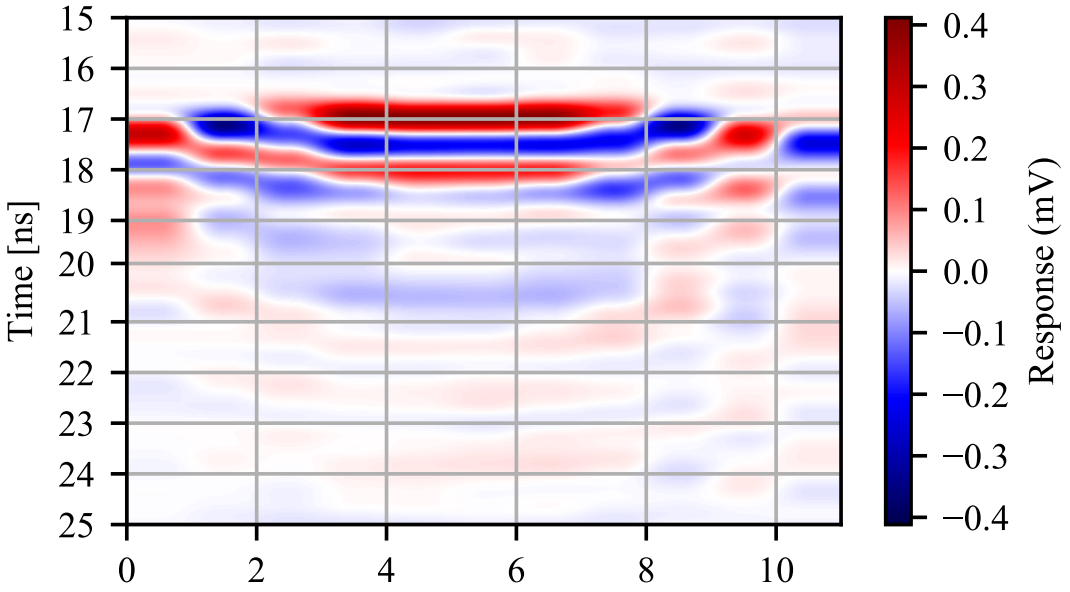

Figure 9.5: B-scan of polarization independent tag over 11 scans interpolated with a Hanning filter where the tag should be at about 22 to 23 ns.

half that of the original co-polarized tag. This may be due to some near field affects not accounted for since the simulation only accounts for a tag that is flat instead of a tag that is conformed against a pipe. The PVC pipe in this situation almost has no response, however the CP tags stand out above the noise. While the long CP tag stands out by also having a possible structural scattering mode, its second pulse is still almost 1 ns longer than the short CP tag. And while the double bowtie tags are not nearly as discernible as the other CP tags, they still provide enough of a response to separate it from the noise. The painted bowtie tag will need to be further investigated as future work to see how much of a response it produces compared to the metal foil bowtie tag. Similarly shown in Fig. 9.8 is the B-scan of a long CP tag, which indicates a strong secondary response, albeit with a smaller delay than the co-polarized tags.

9.2.1 Discussion

In this free space test, comparisons can be made to previous works and the best tag out of this set can be chosen. Overall if both cross polarization tests and co-polarization tests are counted as equals, the cross polarization delay line tags outperform the simple delay line tags. Although the response from the simple delay line tag can be further away from the pipes response, the CP tags have a much greater response over any other objects response, relating back to Shen's experiment with one circularly polarized tag[56]. The major difference being the center frequency and, in this case, that only linearly polarized tags are used. Either way both the previous experiments and this experiment indicate that this can further reduce clutter. For

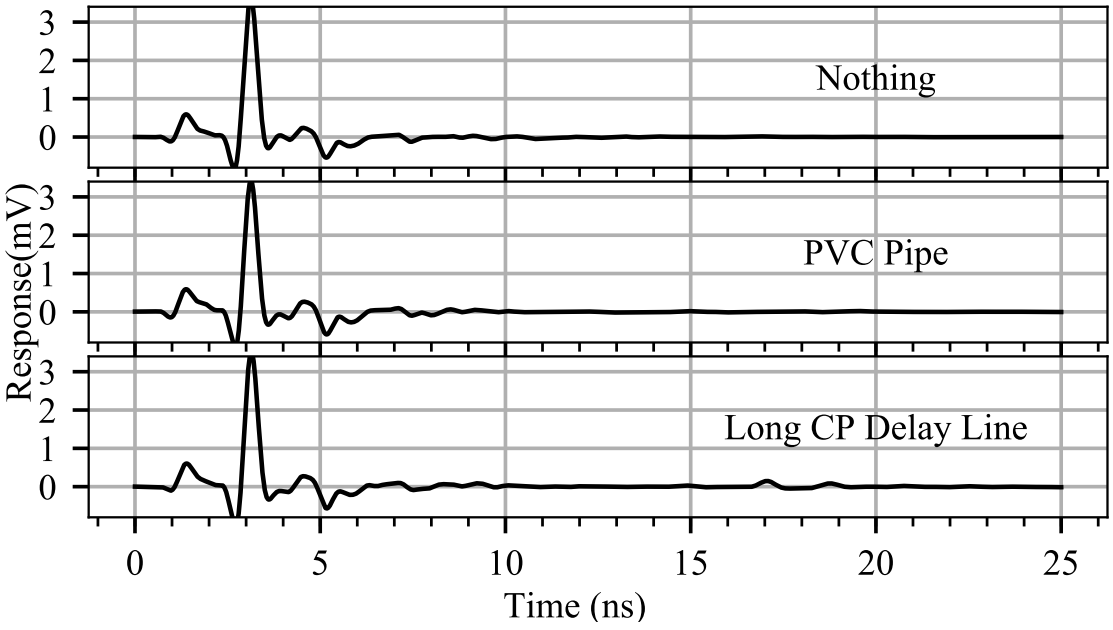

Figure 9.6: Baseline from 0 to 25 ns with antennas in the cross polarization position. Note the strong initial pulse at 4 ns coming directly from the first antenna or shortest path.

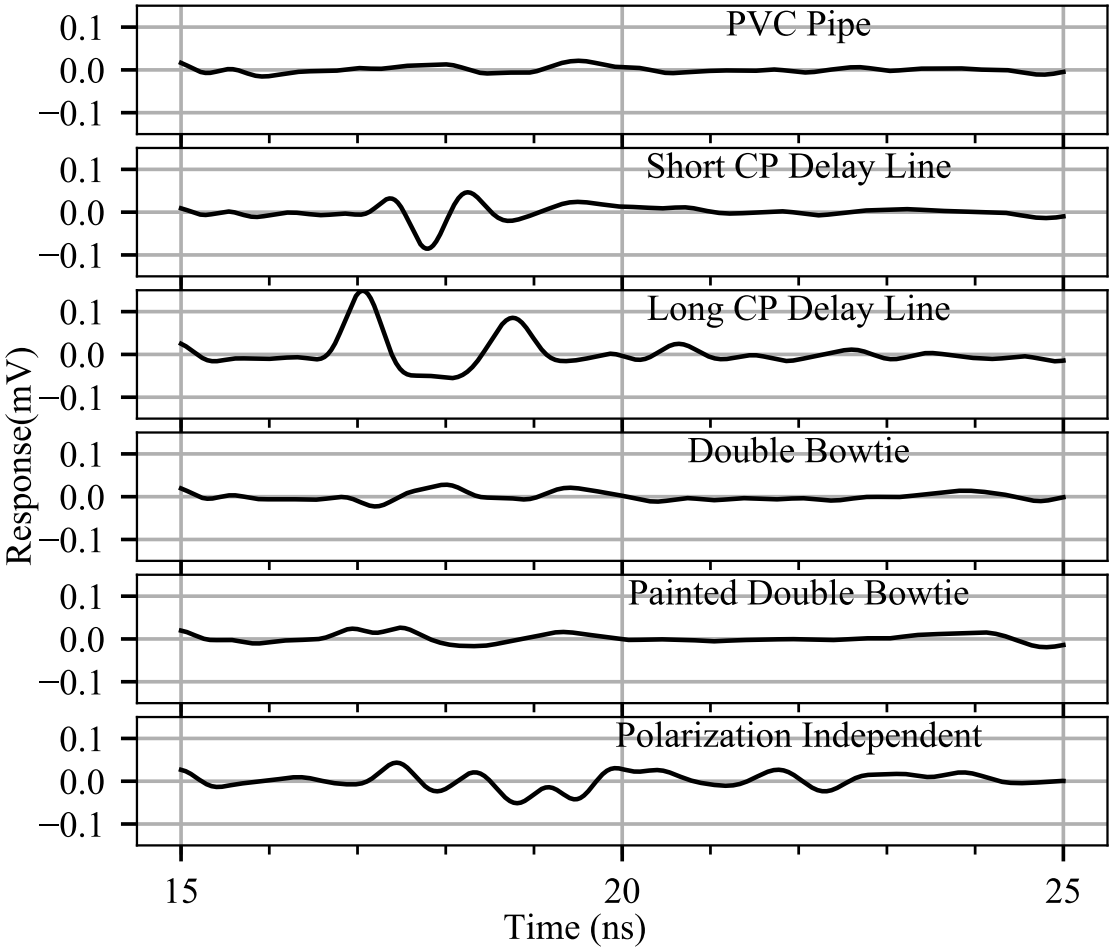

Figure 9.7: A-scans with antennas in cross polarization position.

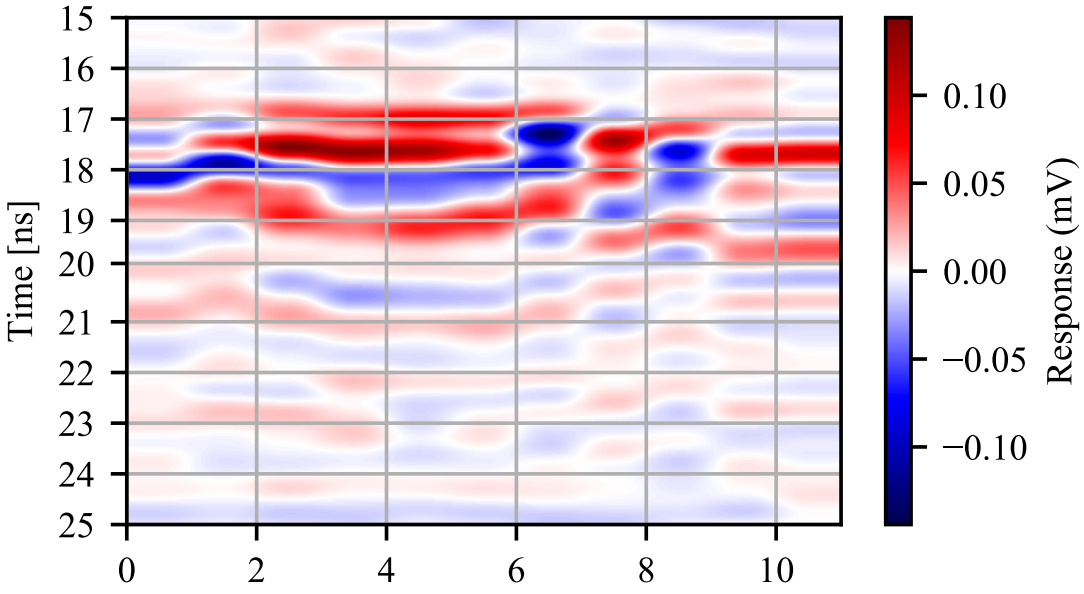

Figure 9.8: B-scan of long cross polarized tag over 11 scans interpolated with a Hanning filter.

the bowtie tags, although they may have been seen, these tags do not have the clear response like Feng's multi-bit angle based chipless RFID tags which even used antennas with smaller bandwidths [26]. The simple delay line tags, compared to Dardari's and Dey's experiments, work just as well as expected even with the larger initial response from the PVC pipe [22, 23].